**ALMA MATER STUDIORUM - UNIVERSITÀ DI BOLOGNA**

**SCUOLA DI INGEGNERIA E ARCHITETTURA**

*DIPARTIMENTO DI INGEGNERIA INDUSTRIALE*

*CORSO DI LAUREA MAGISTRALE IN INGEGNERIA ENERGETICA*

**TESI DI LAUREA**

in
Impatto Ambientale dei Sistemi Energetici M

# ANALISI E SIMULATIONE DI UN CICLO RANKINE ORGANICO PER IL RECUPERO DI ENERGIA A BASSA ENTALPIA

CANDIDATO:
Marco Fragai

RELATORE:
Chiar.mo Prof. Andrea De Pascale

CORRELATORE
Steven Lecompte

Anno Accademico 2015/16

Sessione III

# Analysis and simulation of an organic Rankine cycle for low-grade heat recovery.

Marco Fragai

# Contents

# List of Figures

# List of Tables

# List of Symbols

| Symbol | Units | Description |
|---|---|---|
| $r_v$ | $-$ | Volume ratio |
| $r_p$ | $-$ | Pressure ratio |
| $P$ | Pa | Pressure |
| $v$ | $m^3/kg$ | Specific volume |
| $w$ | J/kg | Specific work |
| $W$ | J | Work |
| $h$ | J/kg/K | Specific enthalpy or heat transfer coefficient |
| $V_s$ | $m^3$ | Expander swept volume |
| $u$ | m/s | Flow velocity |
| $\dot{m}$ | kg/s | Mass flow rate |
| $N_{rot}$ | $rpm$ | Rotational speed |
| $Re$ | $-$ | Reynolds number |
| $Pr$ | $-$ Prandtl number | |
| $Nu$ | $-$ | Nusselt number |
| $U$ | $W/m^2K$ | Overall heat transfer coefficient |
| $A$ | $m^2$ | Area |
| $A_{exch}$ | $m^2$ | Heat transfer area |
| $Q_{amb}$ | J | Heat losses |
| $Q$ | J | Thermal power |
| $V$ | $m^3/h$ | Volumetric flow rate |
| $SC$ | $°C$ | Sub-cooling |
| $SH$ | $°C$ | Super-heating |
| **Greek symbols** | | |
| $\beta$ | $-$ | Chevron angle |
| $\varepsilon_s$ | $-$ | Isentropic efficiency or heat exchanger effectiveness |

| | | |
|---|---|---|
| $\mu$ | Pa s | Dynamic viscosity |
| $\rho$ | kg/m$^3$ | Density |
| $\xi$ | $-$ | Friction factor |

### Subscripts

| | |
|---|---|
| $su$ | supply |
| $ex$ | exhaust |
| $s$ | isentropic |
| $nom$ | nominal |
| $d$ | Design |
| $EVAP$ | Evaporator |
| $COND$ | Condenser |
| $E$ | Expander |
| $P$ | Pump |
| $CF$ | Cooling fluid |
| $HF$ | Heating fluid |
| $WF$ | Working fluid |
| $in$ | Inlet |
| $out$ | Outlet |
| $evap$ | Evaporating |

## Acronyms

**ORC** Organic Rankine Cycle

**CHP** Combined Heat and Power

**PV** Photovoltaic

**CSP** Concentrated Solar Power

**TFC** Total Final Consumption

**ODP** Ozone Depletion Potential

**GWP** Global Warming Potential

**PI** Proportional Integer

**CFM** Coriolis flow meter

# Chapter 1

# Introduction to ORC technology

In order to introduce this work the current energy scenario and Organic Rankine Cycle (ORC) characteristics will be presented in this chapter. This overview is meant to outline the important role represented by the ORC cycle in the energy saving scenario and to clarify the scope of this work. In particular the last section introduces the focus on the numerical simulation of these power plants.

## 1.1 The importance of energy saving in the current scenario.

Over the past decades the world energy consumption has been rising due to population growth and bigger energy intensity of buildings and industry. This consumption is associated with a releasing of large quantities of $CO_2$ and other polluting substances into the atmosphere [2] . Growing concerns over climate change have called for measures to reduce green house gases emissions, these include:

- A decrease in the energy intensity of buildings, industry and transportation.
- A shift from fossil fuels toward clean power generation through renewable energies, comprising wind energy, PV, CSP, biomass, geothermal and large hydro.
- A smarter and more efficient use of the energy sources.

According to a recent study, realised by the International Energy Agency IEA [64], consumers in the member countries have saved USD 5.7 trillion over

the last 25 years, as a result of energy efficiency investments that avoided 256 exajoules (EJ) of Total Final Consumption (TFC). TFC is defined as the sum of consumption by the different end-use sectors. Energy efficiency investments avoided the consumption of 22 EJ or 520 million tonnes of oil equivalent (Mtoe) in 2014, which exceeded the annual TFC in Japan and Korea combined. This "virtual supply" represented by the energy saved through efficiency policy, is competing with oil, gas, electricity and other more traditional elements of TFC. Moreover it has a valuable impact on the fossil fuels dependence and on the pollution issue. For these reasons, investments in energy efficiency will probably keep growing, despite lower oil and gas prices.

## 1.2 The ORC technology

In this scenario the organic Rankine cycle technology appears to be very promising for energy saving. In fact it can be successfully applied to generate power from different low-temperature heat sources ($< 350°$ C), representing an interesting solution for the purposes presented above. For instance, installing an ORC to convert waste heat into electricity enables a better use of the primary energy in industry and residential applications, reducing the energy intensity. This approach is known as Combined Heat and Power (CHP) [32]. Moreover, the low temperatures required for this technology allows converting renewable heat sources into electricity.
The applications of this technology will be further discussed in paragraph 1.2.3.

### 1.2.1 Cycle structure

The structure of an organic Rankine cycle corresponds closely to that of the steam Rankine cycle, except some differences can be noted; the major one is the working fluid, which is an organic compound replacing the conventionally used water. This liquid is vaporized in the evaporator and then expanded in a turbine, to produce mechanical work. The turbine is then coupled to a generator to produce electricity. The expanded working fluid, which usually is still a superheated vapour, is cooled and condensed in the condenser and subsequently pumped back to the evaporator, to complete the cycle.
The conventional representation of the plant is shown in 1.1a. On the left of the figure is presented the conceptual scheme, while the T-S diagram, with the corresponding points, is on the right.

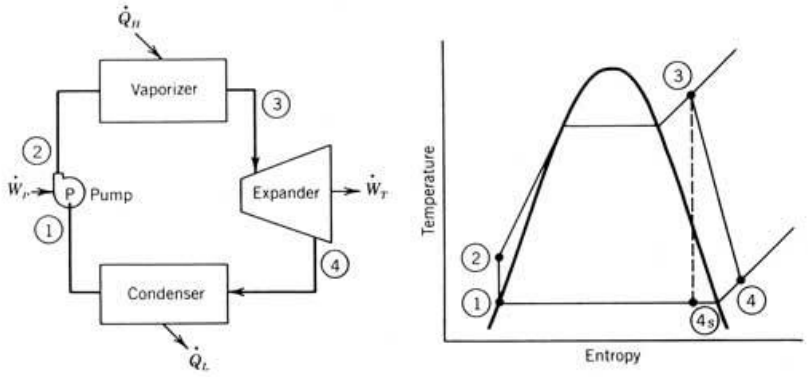


(a) Simple cycle

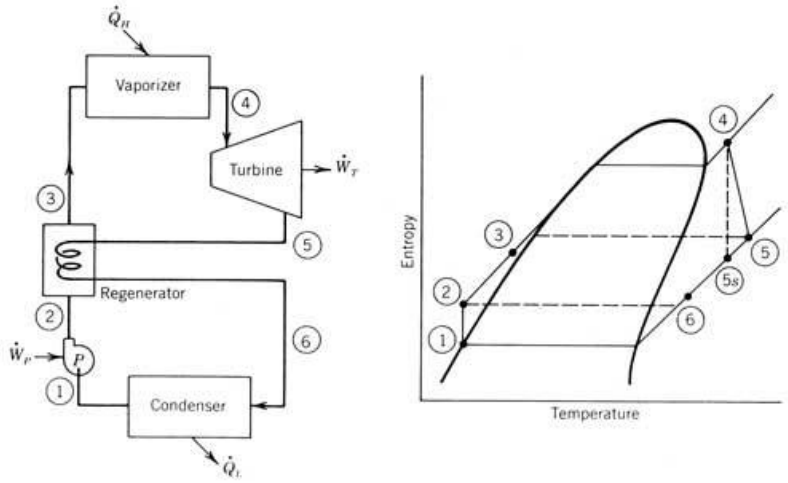


(b) Recuperated cycle

Figure 1.1: Schematic view and TS diagram for two basic cycles [61]

A variation often used includes a recuperator heat exchanger; this configuration allows reusing the heat after the expander to preheat the working fluid and, essentially, increases the thermal efficiency [38]. The scheme and TS diagram are represented in 1.1b. Variations in the cycle architecture such as reheating and turbine bleeding are generally not common in ORC systems [53].

### 1.2.2 Fluid selection

As we stated above, the working fluid used in the cycle is the most important difference between ORC and the conventional steam power plant. In fact, in order to exploit low-temperature thermal sources with a classical steam

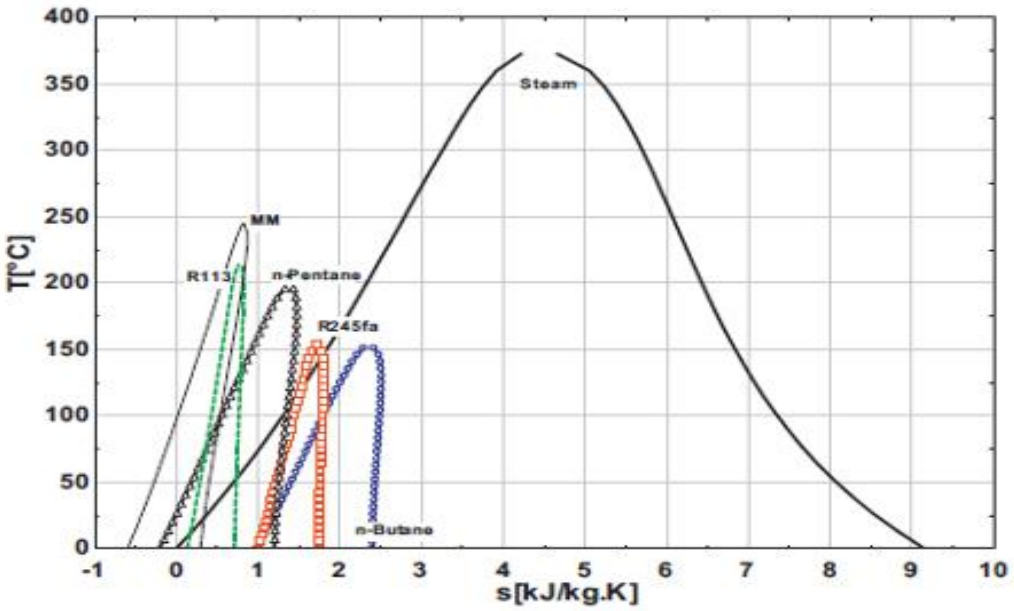


Figure 1.2: T-s diagram comparison for water and some organic fluids [62].

cycle, some important problems would arise [62]:

- Need of superheating to prevent condensation during expansion
- Risk of erosion of turbine blades, which leads to complex and expensive turbines
- Excess pressure in the evaporator.

Part of these issues can be mitigated using an organic compound, characterized by higher molecular mass and lower boiling/critical temperature than water. The organic cycle has thus the following features [62] [8]:

- The evaporation process takes place at lower pressure and temperature.
- The expansion process ends in the vapour region and hence the superheating is not required and the risk of blades erosion is avoided.
- The smaller temperature difference between evaporation, and condensation also means that the pressure drop/ratio will be much smaller and thus simple single-stage turbines can be used; this means less expensive and more simple machines.

The T-s curves of some organic compounds are compared to water in 1.2..

A working fluid must have the necessary thermo-physical properties that match the application, but should furthermore also have adequate stability in the desired temperature range [5]. The fluid selection affects system efficiency, operating conditions, environmental impact, and economic viability. For this reason the selection of the working fluid is one of the most important aspects in the design of the power plant [52]. This justifies the abundant literature dedicated to fluids selection for very different heat recovery applications. The main physical and chemical features considered for this choice are:

**Type of fluid:** A working fluid can be classified as a dry, isotropic, or wet fluid depending on the slope of the saturation vapour curve on a T-S diagram (dT/ds). When the value of the slope is positive the fluid is called dry (e.g. pentene), wet for a negative value (e.g. water) and isentropic fluid with nearly infinitely large slopes (e.g.R11).

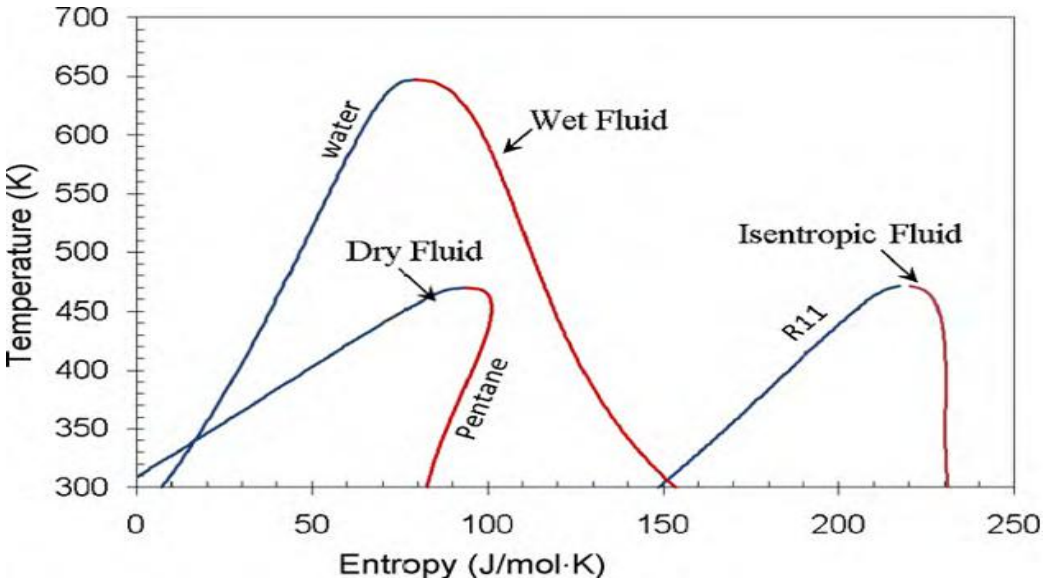


Figure 1.3: Different types of fluid [17].

A positive slope allows the saturated vapour at the turbine inlet to remain saturated throughout the turbine exhaust, without condensation. As a consequence, there is no need for installing a regenerator, reducing the cost and making these fluids very suitable for ORCs [21]. However if the fluid is "too dry," the expanded vapour could be too superheated, which increases the cooling load in the condenser; in this case a regenerator is needed, increasing the system's investment cost and complexity.

**Thermodynamic main parameters:** One of the most important factors is the latent heat. Maizza et al. [44] suggest the use of high density and high latent heat fluids, to absorb more energy from the source in the evaporator, and thus reduce the required flow rate, the size of the facility, and the pump consumption. Chen et al. [17] found that fluids with higher latent heat produce larger unit work output, when the temperatures and other parameters are defined. However, when the heat source is the waste heat, organic fluids with lower specific vaporization heat are preferred. That's because the temperature profile of the working fluid in the evaporator better follows the temperature profile of heating fluid in the heat source; hence, the irreversibility in the heat transfer process is decreased [36]. Another important parameter is the critical point. This influences the range of operating temperature and pressure. In a subcritical cycle the critical temperature of the working fluid should at least be higher than the ambient temperature in order to allow for heat rejection by condensation. Furthermore the evaporation process occurs at a lower temperature than the critical temperature. In contrast, for a transcritical cycle the working fluid achieves a higher temperature and pressure than the critical values. The ratio between the working pressure and the critical pressure also influences the density, and thus the sizing and performances of the cycle.

**Others parameters** of interest are: the molecular weight, which could influence the heat transfer properties and the expander behaviour, the environmental impact, measured in terms of Ozone Depletion Potential (ODP) and Global Warming Potential (GWP), cost, availability and safety.

### 1.2.3 Applications

In the framework of waste heat and renewable heat sources, ORC technology offers an interesting option. In fact, ORC system can be used, with little modifications, in conjunction with various heat sources. Moreover, unlike conventional power cycles, this technology allows decentralized and small scale power generation, even for low temperature heat sources. Other technical advantages are: long service life, low maintenance costs, fully automatic and unmanned operation, improved part-load characteristics, etc.
Some examples of application can be found in the following fields:

**Biomass:** Biomass can consist of several natural resources ranging from wood to agricultural waste. The application of ORC technology is

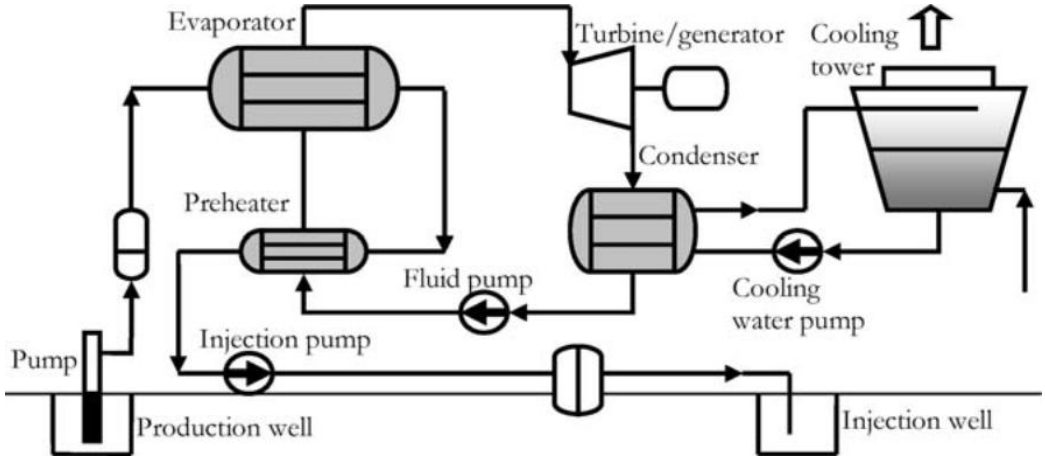


Figure 1.4: Flow diagram for a binary geothermal power plant [62].

becoming mature and cost-effective in this field, and the number of installed plants is rapidly increasing, especially in micro and small-scale CHP [23]. A typical system is made-up of a biomass-feed boiler and an Organic Rankine Cycle module, coupled via a thermal oil loop. The thermal oil used as heat transfer medium provides a number of advantages, including low pressure in the boiler, large inertia, simple control and operation. The condensation heat can be used to produce hot water, suitable for district heating and other thermal processes, such as wood drying and sorption cooling. Biomass ORC CHP plants at medium scale (100–1500kW) have been successfully demonstrated and are now commercially available [55], while small scale systems of few kW are still under development [42].

**Geothermal energy** Organic Rankine cycle has been proposed also as an efficient technology for converting the low- and medium-temperature geothermal heat to electricity. There are several advantages in using an ORC, compared to conventional steam power cycles, including more efficient utilization of energy resource, smaller systems and outstanding economical performance [57]. Geothermal heat sources are available over a wide range of temperatures, between 120° and 300° C. To recover heat at an acceptable temperature, boreholes must be drilled in the ground. The hot brine is extracted from the production well, passes through the ORC evaporator and is pumped back in the injection well, as shown in 1.4.

In geothermal plants the auxiliary consumption could be relatively high, and the working fluid selection together with the cycle optimiza-

tion are really important challenges. The cycle performance is usually evaluated as energy and exergy efficiency. First law efficiencies are found in the range 5–15% while second law efficiencies are typically in the range 20–54% [22]. A large number of studies defines criteria and guidelines for the optimal design of binary cycle power plants (e.g. [6] and [14]) and fluid selection (e.g. [57] and [26]), using different optimum criteria. Anyhow, untill now, there is no prominent criterion recognised. From a theoretical point of view, a transcritical cycles could increase the cycle performance, because better matches with the heat source and cold sink profiles, but safety and condensation problems may arise [27].

**Waste heat recovery (WHR)** In many industrial processes excess heat needs to be rejected. If this heat is unused and directly dumped into the atmosphere we speak of waste heat. One example is the cement industry, where 40% of the available heat is expelled through flue gases [16]. This energy often cannot be reintegrated on-site, and is therefore rejected to the atmosphere. The use of this rejected energy as the heat source inside an evaporator represents a promising application for ORC technology. In fact, in Europe a potential of 3000 MWe is estimated for power generation from industrial waste heat [9]. Another heat recovery application can be found in internal combustion engines, especially the stationary applications. A ICE typically converts about one-third of the fuel energy into mechanical power, and an ORC system could reuse some energy from exhaust gases or from the cooling circuit. Some examples of stationary ICE applications can be found in biogas engines [34] and diesel engines [34]; however the majority of studies present in literature are just thermodinamic and techno-economic analyses [65] and [63] . Few examples of ORCs coupled to mobile ICEs exist and they are usually prototypes [24].

Many other applications are currently being studied, mainly in the form of prototypes or proof-of-concepts. These innovative applications include: modular organic Rankine cycle solar systems [3], ocean thermal energy conversion systems [25], solar ORC-Reverse osmosis desalination systems [20], automotive, and shipping industry [1]. A basic idea of the main fields of application of ORC technology can be summarized in figure 1.5. As shown in the figure above, the biomass-powered ORC is the most common and mature use, WHR and geothermal are pretty frequent, while solar applications are still very rare.

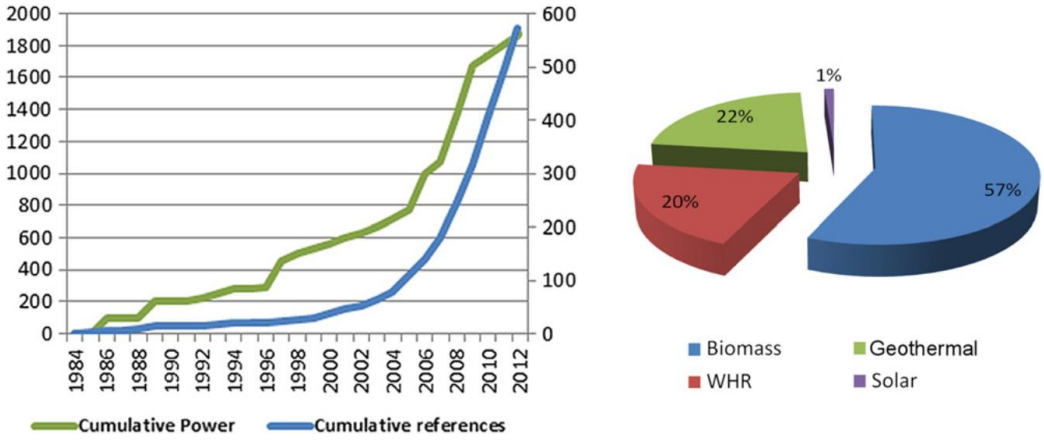


Figure 1.5: Share of each application in terms of number of units, 2012 [53].

## 1.3 Motivation and Scope

As we have outlined in the previous sections, the organic Rankine cycle is a relatively new and expanding technology. New applications and new architectures are being studied and both the cycle structure and its features are far from being defined. New ideas are applied every day to find more efficient and cost-effective solutions, in order to open new scenarios in energy efficiency applications.

This goes together with the usual, fundamental influence of the components of the cycle itself. In fact, as we will discuss later, many different alternatives are under investigation for expander sand heat exchangers. These components have great influence on the performance of the power plant, and they need to be developed and tested.
Moreover, we have outlined the importance of the working fluid selection in this technology; its great influence on performance makes the working fluid another important aspect to investigate. Anyway, a theoretical study is usually not suitable or sufficient to evaluate a new component or a different architecture; nor to optimize the match between the working fluid and the power plant.

A strong need for experimentation is thus emerging, in order to collect new data and to test different solutions. Unfortunately, perform real experiments is often very expensive and time-consuming, so the use of computer simulations is becoming more and more important and wide spread.
For all the aforementioned reasons, these computer simulations should be as more complete and reliable as possible. In a research field they can represent a valuable tool to investigate new components and configurations, and they

can also optimize a given plant in an industrial environment.

Therefore, the main focus of this work is on the computer simulations of ORC systems. We will start from a theoretical study of the main components and their models, trying to create a MATLAB code of every model. Each simulation will be compared to the data from the test power plant, available in Kortrijk. The main goal is to build and validate a model of the whole ORC system.

# Chapter 2

# Test bench and experimentation

Before we present the detailed modelling for every element, a brief description of the experimental test bench is provided.
The ORC test bench used in the experiments is located at Campus Kortrijk of Ghent University. The test-bench consists of four main components: the expander, pump, evaporator and condenser. In addition, a recuperator which can be bypassed is added to increase the thermal efficiency of the cycle. A liquid receiver is also present, in order to prevent pump cavitation. The initial cycle was built by *BEP Europe* but it was later modified for study purposes. Figure 2.1 shows a schematic view of the plant, while 2.2 is a picture of the test rig.

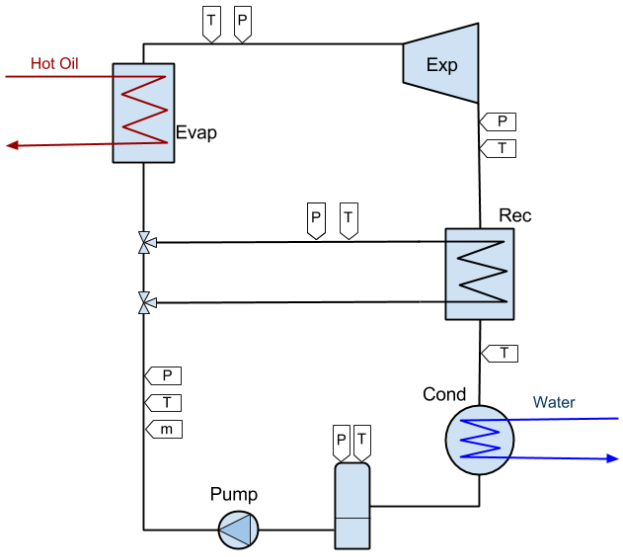


Figure 2.1: Schematic representation of the plant.

Figure 2.2: Front view of the test bench

## 2.1 Test bench features

The main elements of the ORC installation are:

**External loops** The thermal energy source is provided by an electrical boiler consisting of ten heating elements, it has a thermal power of 250 kW that can be smoothly varied from 0 to 100%. *Therminol66* is selected as heating fluid and is pumped through the evaporator. The advantage of this oil-type boiler is that the heat source loop remains unpressurized within the whole temperature range of temperature, up to 350° C.
A Proportional Integer (PI) controller is implemented to maintain constant the temperature of the oil entering the evaporator. The heating fluid mass flow rate can be changed adjusting the pump speed. A manual control strategy can be selected to control the transferred power; anyhow this strategy could be hard to handle in some particular situations, because it could lead to unstable behaviour.

The cooling fluid is glycol water, which is pumped through the condenser; the water is then cooled down by means of a dry air cooler with

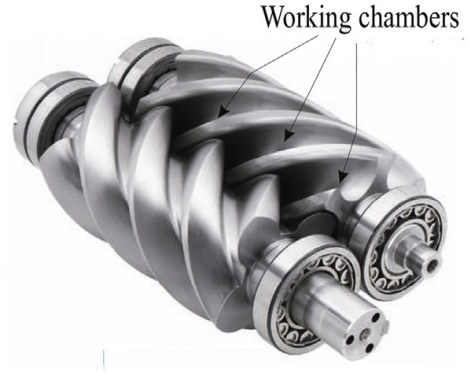


Figure 2.3: Twin expander rotor [49].

480 kW nominal capacity at 60° C difference with the ambient temperature. There is also a three-way valve to simulate different temperature profiles. Anyhow we have not used this control in our experiments. The flow meter is of ultrasonic type with an accuracy of 0.05% within the design region; the measured volume flow rate is recalculated to a mass flow rate based on the mixture properties as a function of the glycol concentration and the solution temperature.

**Expander** Different expanders have been tested in this plant. The initial expander was a 11 kW singe-screw model but it has been replaced by a twin-screw machine. The expander used for this study has a 4/6 lobe (male/female) arrangement with a nominal operating speed of 6000 rpm, a 8 kW nominal power and a pressure ratio equal to 6. The twin-screw is represented in figure 2.3.

**Heat exchangers** The heat exchangers used for evaporator, recuperator and condenser are identical. They are brazed plate heat exchangers manufactured by the company *SWEP* [4]. The evaporator is insulated with a glass wool layer of 180 mm thickness. The technical features of these devices are presented in Table 2.1

| Model | SWEP B200T SC-M |
|---|---|
| Number of plates | 150 |
| Dimensions [mm] | 525 x 353x 243 |
| Maximal Pressure [bar] | 45 at 135° C |

Table 2.1: Technical features

Table 2.2: Characteristics of measurement devices

| Variable | Device | Range | Uncertainty |
|---|---|---|---|
| T (wf) | RTD | $50 - 300°$ C | $\pm 0.2°$ C |
| T (oil) | RTD | $30 - 350°$ C | $\pm 0.2°$ C |
| T (water) | RTD | $0 - 150°$ C | $\pm 0.2°$ C |
| Mass flow | CFM | 0 - 1.8 kg/s | $\pm 0.09\%$ |
| Pressure | APS | 0 - 16 bar | $\pm 0.016$ bar |
| El. Power | Wattmeter | $0 - 100$ GW | $\pm 0.1\%$ |
| Rot. Speed | Tachometer | $3 - 99999$ rpm | $\pm 1$ rpm |

**Pump and fluid** The model of turbopump used in the cycle is *Calpeda MXV 24-214*, with 14 stages. It has a nominal power of 2.2 kW, 2900 *rpm* nominal speed and a maximum head of 149 m at 4.5 $m^3/h$.

The working fluid adopted, the R245fa, is a common refrigerant used in ORC systems [53]. It is characterized by a positive slope of the saturated vapour line in the T-s diagram which will prevent the formation of liquid droplets at the exit of the expander.
The physical properties of all the fluids used in the calculations are obtained using the free library *CoolProp* developed by Bell et al. [11].

**Data acquisition** Absolute pressure sensor (APS) and resistance temperature detectors (RTD) at the inlet and at the outlet of the different components allow the determination of the energy balance for each component. In the scheme 2.1 the pressure and temperature measurements are represented using flags with the letter $P$ and $T$ respectively. The mass flow rate is measured by means of a Coriolis flow meter (CFM) installed at the turbo-pump outlet. The cooling loop is equipped with two RTDs to measure the temperature of the cooling fluid at the inlet and at the outlet of the condenser and an ultrasonic flow-meter is used to measure the flow rate of glycol water. In the heating loop, the temperature of *Therminol66* is measured at the inlet and at the outlet of the evaporator and a pressure difference transmitter is used to calculate the oil mass flow. The electrical power at the generator outlet is measured by means of a wattmeter. The characteristics of the measurement devices are reported in Table 2.2.

## 2.2 Test campaigns

A lot of data were already available for this plant. Anyhow they were rather rough and difficult to analyse. For this reason the first part of the work consisted in the study of the entire set of data, in order to identify the most relevant information.
The second part of data collection was a brand new campaign. The aim of this work was the collection of more steady-state data to validate the simple ORC model that we were creating. In fact, it was crucial to develop and test the models on a complete set of heating and cooling conditions.

All the test data are the result of the great work of all the researchers at Kortrijk campus, such as Sergei Gusev, J. Andres Hernandez Naranjo, Martijn van den Broek and others. They were all really kind and helped me a lot with the tests. A complete view of control panel of the power plant is given in Appendix 1.

### 2.2.1 Analysis of the first data set

The data from the former experimentations were a continuous registration of all the sensors of the cycle, for every instant of time. Since the focus of this thesis is the steady-state behaviour, we decided to create a Matlab code able to distinguish the steady state from the unsteady one. The criteria used to define the steady-state are the same proposed by Woodland et al. [66], i.e. a steady state is automatically detected if within 10 minutes the deviation of the following parameters is smaller than:

Temperature Difference $< 0.5°$ C;

Pressure Change $< 2\%$;

Mass Flow Change $< 2$ %;

Rotating Equipment Speed Change $< 2\%$.

The time required for the measured temperatures and pressures in the condenser to stabilize is longer than for all other operating parameters, therefore these temperatures are taken as indicators of a steady state.

Anyway the variation limit of 2% appeared to be very severe for the mass flow rate and it was almost never respected. Therefore we decided to set a limit of 4% for this variable. Moreover, also the size of the interval, in which the analysis is performed, turned out to be very strict. In fact, in our data the inputs are changed pretty often and almost no steady state interval is

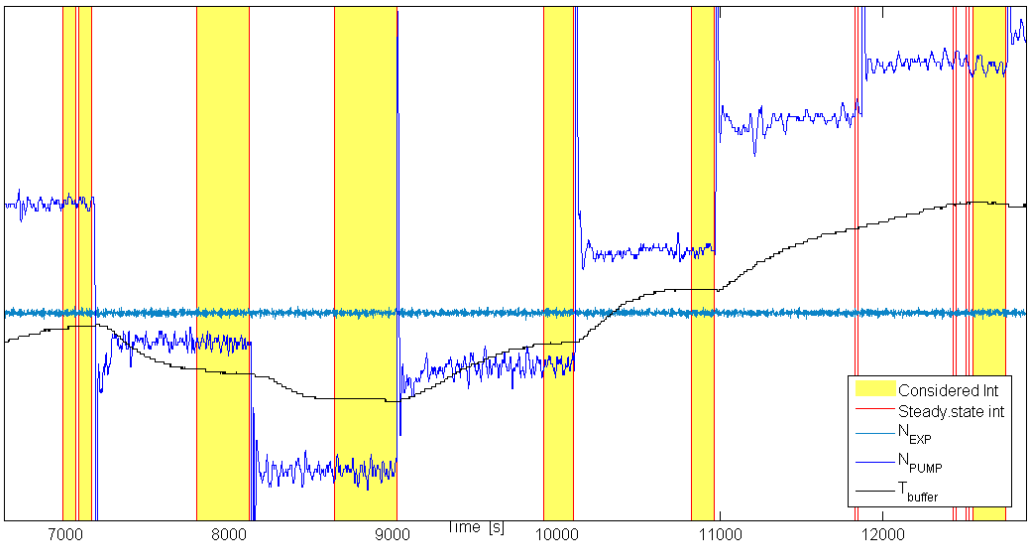


Figure 2.4: Steady-state identification

long enough to fulfil this requirement. Therefore we set the interval length to 300 s .

The Matlab script, based on these criteria, analyses every second of data and finds the steady-state points. The results obtained for one set of data are shown in Figure 2.4. Every steady-state interval is marked using two red lines. Not all the steady-state intervals are considered meaningful, the smallest (less then 50 s) are neglected, the others are marked in yellow. On the background of the figure are also represented the qualitative trend of the main operating parameters; this in order to confirm the achievement of a steady behaviour. The result of the script is thus a table containing, for every interval considered in steady-state, the value of the operative parameters of the cycle. The list of the experiment is quite long, so we decide to present in Table2.3 only the maximum and minimum value of each variable.

Another function included in the Matlab script is the possibility to draw the *T-s* diagram for every steady-state point. In fact, this figure represents a quick glimpse of the cycle and can be really useful in its analysis. The numbers in the example diagram represented in Figure 2.5, are referred to the scheme 2.1.

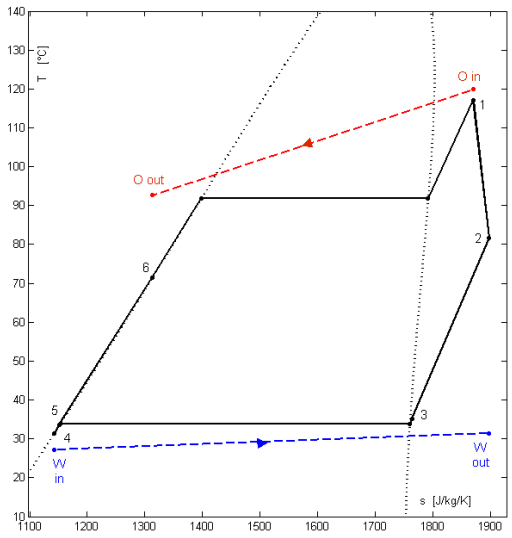


Figure 2.5: T-s diagram

Table 2.3: Test conditions resuming table

| | $min - max$ | | $min - max$ |
|---|---|---|---|
| $m_{oil}$ | $1.29 - 1.84\ kg/s$ | $T_{oil}\ in$ | $108 - 130°$ C |
| $V_{water}$ | $13.2 - 17.1\ m^3/h$ | $T_{water}\ in$ | $17.7 - 40.1°$ C |
| $N_{rot}\ exp$ | $1500 - 8000 rpm$ | Exp Power | $0.75 - 6.94\ kW$ |
| $m_{wf}$ | $0.18 - 0.38\ kg/s$ | SH | $12.5 - 38.5°$ C |

### 2.2.2 Second test campaign

The second campaign of test was entirely focused on the validation of my model. The main goal of this data collection was investigating the behaviour of the cycle in the simple configuration, without the recuperator. In fact, all the data collected in the previous experiments were based on the recuperated configuration. During these tests I had the possibility to visit the test bench and work on the plant alongside the researchers in Kortrijk, in particular Sergei Gusev.

All the data were collected in the following conditions: steady-state regime, without recuperator and for a constant rotational speed of the expander. Many different conditions have been tested for the heating and cooling loops and for the superheating; this in order to have various points to evaluate the performance of the simulation model.

However the collection of these data was not so easy to achieve. Indeed, the automatic control system was calibrated on the recuperated architecture and showed some problems in the simple configuration. A patient effort was thus needed to adjust all the cycle parameters manually and avoid instability. For the aforementioned reasons, it was not possible to obtain stable and valid results in all the points that we decided to investigate at the beginning. The tested conditions are resumed in Table 2.4 and 2.5. In particular we chose to operate the expander at the nominal speed of 5000 *rpm* and use two levels of super-heating: 10 and 20° C. This choice for the super-heating is the result of the compromise between two requirements: using two values as different as possible and limiting the pressure of the lubrication system. The mass flow rate of the oil had to be changed in the second experiment. In fact, using a smaller super-heating, the value of 3 kg/s resulted in an excessive evaporating pressure; the chosen value was thus 2.1 kg/s.

| SH | Input param | Values |
|---|---|---|
| 10° C | $m_{oil}$ | 1.5 |
| | | 2.1 |
| | $V_{water}$ | 7 |
| | | 13.4 |
| | | 19.7 |
| | $Toil_{in}$ | 120 |

Table 2.4: Test 1

| SH | Input param | Values |
|---|---|---|
| 20° C | $m_{oil}$ | 1.5 |
| | | 3 |
| | $V_{water}$ | 7 |
| | | 13.4 |
| | | 19.7 |
| | $Toil_{in}$ | 110 |
| | | 120 |

Table 2.5: Test 2

# Chapter 3

# Expander analysis and simulation

Since our main goal is the computer simulation of a complete and general cycle, we need to study every component thoroughly. In particular we decided to focus on heat exchangers and expander, since they have a dominant role in the plant. For each element we present:

- brief description of the main features of the component,
- different technologies applied in the ORC technology,
- the essentials models adopted in its study,
- modelling and validation.

The goal of this approach is gaining a deep understanding of the features of every element and thus, be able to chose the most suitable model in the modelling phase.

## 3.1 Introduction

In a ORC system the expander is the core component and has a crucial role in the overall system performance. Two main types of expanders are applied in ORC, they can be classified into two types:

1. the *velocity type*, such as axial turbines and radial-flow turbines;
2. *positive-displacement type*, such as scroll expanders, screw expanders and piston expanders.

Overall mechanical or electrical efficiency depends on the match between expander characteristics, fluid properties and operating parameters of the thermodynamic cycle.

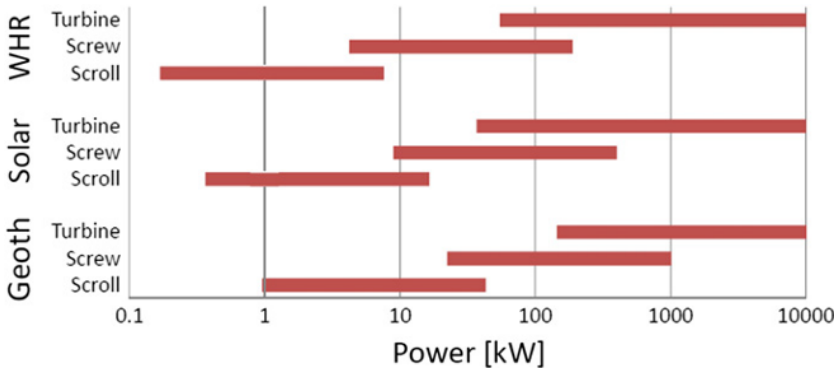


Figure 3.1: Range of application for different expander technologies and applications, from [53].

Turbine expanders are usually applied in relatively large-scale systems with an output power above 50 kW [53]. In fact, turbine expanders are not suitable for small scale units, mainly because their rotational speed increases exponentially with the decrease in turbine output power. Furthermore, a small-scale turbine expander is expensive and not commercially viable.

The positive displacement expanders are more appropriate to the ORC-based micro- CHP units because they are characterized by lower flow rates, higher pressure ratios and much lower rotational speeds compared with the velocity-type expanders [19]. However, volumetric expanders are generally less convenient to high expansion ratios, compared to turbomachines; in fact, they exhibit greater losses include friction, supply pressure drop, internal leakage and heat transfers [58]. The major types of positive displacement expanders are piston, scroll and screw expanders. The rotary expanders are far more common than reciprocating piston expander because of various advantages such as:

- The absence of valves, the timing of suction and discharge is imposed by the geometry of the machine;
- Less moving parts, resulting in better reliability;
- The fact that suction and discharge do not occur in the same location limits the suction heat transfer, which has a positive impact on the volumetric performance of the machine.

The figure 3.1, represent a typical range of application for different technologies and heat source, from Quoilin et al. [53].

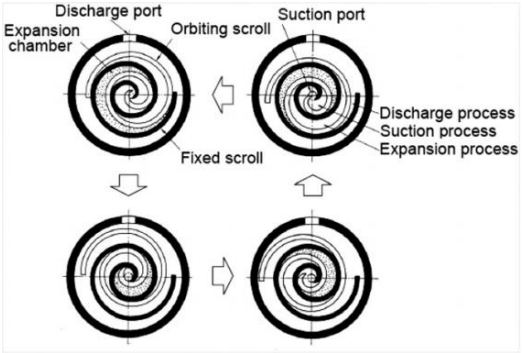


Figure 3.2: Scroll expander model [54].

## 3.2 Expander technology

In this section are resumed the main features of the three most common technologies.

### 3.2.1 Scroll expanders

Among positive displacement machines, the scroll machine is a good candidate for the ORC application, because of its reduced number of moving parts, reliability, wide output power range, and broad availability. Moreover, it is a proven technology because over the past few decades, scroll machines have been widely used in the fields of air conditioning and refrigeration.
Currently, the majority of scroll expanders integrated into the low-grade energy utilization systems are modified scroll compressors.

A scroll expander is made up of two identical involutes which form right- and left-hand components. The two scrolls are coupled phased of 180 degrees one respect to the other. This indexing creates crescent-shaped gas pockets, bounded by the involutes and base plates of both scrolls.
In operation, one scroll remains fixed and the other is attached to an eccentric shaft, which drives a generator. The working fluid enters at the centre of the scrolls. As the moving scroll orbits around the fixed scroll, the tiny pockets formed follow the spiral outward and enlarge in size. The entering gas is trapped in two diametrically opposed gas pockets and expands as the pockets move toward the periphery, where the discharge port is located [60]. For a better understanding of the expansion process refer to figure 3.2.

No valves are needed, which reduces noise, losses and improves the durability of the unit. Another interesting feature of this technology is the good dynamic balance that implies nearly no vibration and a continuous power

delivery. The fast growing mass production of such units as compressors is likely to contribute to a lowering of the production costs also for expander applications.

From the point of view of the compressor structure, two configurartions can be identified. The hermetic and open-drive expander.

In the hermetic configuration the components and motor drive are assembled with a common shaft and welded into a steel container. Hermetic and semi-hermetic compressor have traditionally been employed in refrigeration, due to their good performance, simplicity and low heat of compression. Hermetic scrolls are mainly used in small power applications and various experiments of ORC systems integrated with hermetic expanders can be found in literature ([15, 47, 67]). The power output of the plants tested in these articles are between 0.5 and 10 kW, with an isoentropic efficiency between 43% and 83%.

The open-drive scrolls have been widely used in automotive industry for air conditioning and they have a more simple set-up. The electric motor is not sealed inside the case but is driven by the engine shaft, through a belt pulley. Usually there is also a clutch that engages and disengages the power transmission. When this device is used to generate power, this assembly could be used as a connection control between the scroll and the generator. There are however additional friction losses and a direct shaft connection could be preferable. The experimental results of some studies, show a lower isoentropic efficiency, between 47% and 70% [60].

Recently semi-hermetic expanders have been tested, modifying compressors used in air conditioning of hybrid vehicles. For reference see Jradi et al. [33] and Saitoh et al. [54].

### 3.2.2 Screw expanders

Screw-type expanders are positive displacement devices consisting of helical screw rotors. The male and female rotors are separated by narrow clearances (in the order of $50\mu$ m), obtained by bearing and timing gears. In the expander machine the fluid volume trapped between the rotors and the expander housing will increase, causing the rotation of the shaft, until it is expelled from the opposite side of the rotors. Power is transferred between the fluid and the rotor shafts by pressure on the rotors.

Like all other positive displacement devices, the seal is critical to prevent internal leakage. In order to prevent direct contact and achieve a seal between the lobes of each rotor lubrication is needed. For this purpose, the oil could be directly injected inside the device or just used to lubricate the gears,

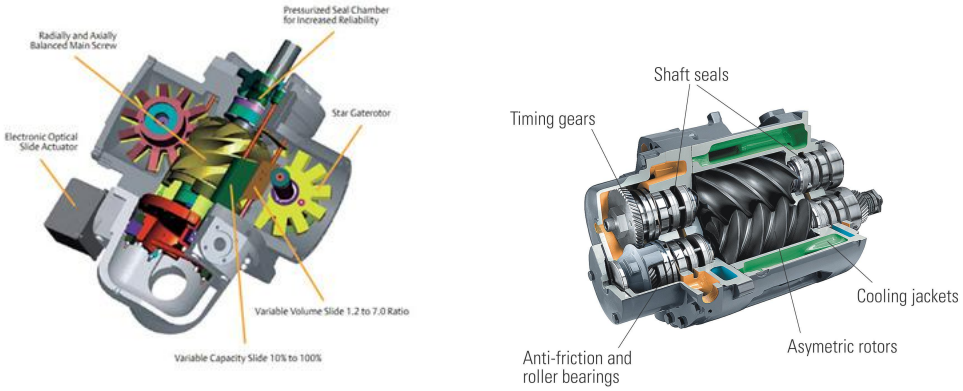


(a) Simple screw expander (b) Double screw expander

Figure 3.3: screw expanders

avoiding the contact with the working fluid (oil-free expander). In the first case an oil separator is required but the machine is pretty simple; on the contrary, an oil-free machine needs seals against the bearings and chamber, making the machine more complicated and more expensive.

There are two types of screw expanders: twin-screw expander and single-screw expander. The single screw expander is composed of a main screw and two gaterotors. Expansion of the gas is accomplished by the engagement of the two gaterotors with the helical grooves in the main screw. The main screw is moved by the expansion of the working fluid between the two elements. The rotational axes of the gaterotors are parallel to each other and mutually perpendicular to the axis of the main screw. A representation is given in 3.3a. In the twin-screw expanders, shown in 3.3b, two mated rotors mesh together, trapping the working fluid, and increasing its volume along the rotors. Twin-screw expander has been widely used in Rankine cycle system.

It has been reported in literature that screw expanders can admit two-phase mixtures to generate electrical power [59] , which makes them suitable for Rankine cycle plants, especially for geothermal and waste heat applications. However screw expanders are not suitable for mechanical power output lower than 10 kW [51]; this due to the difficulty in sealing the organic working fluid.

Compared with the twin-screw expander, the single-screw expander has a longer service life, more balanced loading of the main screw and more simple configuration. Anyhow single-screw expander can cover only a limited range of power, typically between 1 - 200 kW.

Many application of the screw technology to the ORC cycle can be found. In particular Smith at al [35, 39] have developed and investigated screw machines as expanders, even in small scale applications. An intresting application of a single screw expander can be found in the article of Zhang et al. [68], where a dual-loop ORC have been tested to harness the waste heat from an internal combustion diesel engine.

### 3.2.3 Turbines

Compared to the other expander technologies, the turbine offers many advantages, such as its compact structure, small size, light weight, stability and superior efficiency [53]. In fact, thanks to the physical properties of the organic fluids, turbines can be a suitable option even in a power rage where the traditional steam turbines become unattractive and inefficient. One of the reasons is the bigger molar mass of the organic fluids, compared to water. A larger molecular mass leads to a smaller enthalpy drop and thus exists a possibility for designing a single-stage high-velocity ratio turbines with moderate peripheral speed and centrifugal stresses. However, the velocity of sound is bigger and this influences the design of the velocity diagrams, in order to minimize shock losses. Moreover, the density of the working fluids is the bigger; this allows the use of a turbine with smaller overall dimensions, when compared to steam turbines. Ultimately, a compromise should be done between the volume flow ratio and the enthalpy drop, in order to obtain reasonable losses. A single-stage turbine is thus very common when the volume flow ratio is not so high. In this case, it is also difficult to obtain satisfactory heights of the blades and high rotational speeds are required. In case of large flow ratio a multi-stage or a radial turbine can be considered.

For the aforementioned reasons, the majority of the manufacturers (as ORMAT, Turboden, BNI, Adoratec, UTC, etc.) use a turbine expander in medium and large-scale ORC applications. Some large-scale plants have been successfully demonstrated in geothermal field [50],biomass [12] and waste heat recovery [46].

### 3.2.4 Conclusions

There are many parameters to evaluate in the ORC expander selection. The most common ones are: the power output, pressure ratio, efficiency, rotational speed, cost and reliability. A general comparison is often very hard to give, due to the different operating conditions of every experiment. Anyway some particular differences appear quite clearly.

Table 3.1: Examples of ORC plants

| Ref. | Expander | Conditions | Power [kW] | Efficiency [ - ] | Press.Ratio [Pin/Pout] |
|---|---|---|---|---|---|
| Lemort | Scroll | R123, 1170-2260rpm | 0.4 - 1.8 | 42 -65% | 2.75 - 5.4 |
| Mathias | Scroll | R123 | 2.9 | 48.3% | 3 - 8.3 |
| Wang | Scroll | R123a 1000-3600rpm | 0.5 - 0.8 | 70-77% | 2.6 - 4.8 |
| Smith | Screw | R113 1300-3600 rpm | 6- 15 | 48- 76% | 2.1 |
| Wei | Screw | Air, 2800rpm | 5 | 31% | |
| Shuster | Screw | R245 500-2300rpm | 2.2 | 68% | 2 - 6 |
| Yagnoub | Radial Turbine | HFE301, 6000rpm | 1.5 | 85% | 1.1 |
| Innoue | Radial Turbine | TFE 15000-30000rpm | 5- 10 | 70-85% | 4.8 |
| Kang | Radial Turbine | r245, 63000rpm | 32.7 | 79% | 4.1 |

The table 3.1 resume the data obtained from different experimentations in literature [10, 51, 53] :

The turbine technology is the most suitable for large capacity systems (the size of the plants reported previously is usually low because most of the research is conducted in a laboratory). Screw expanders can adequately fit the medium range power and scroll expanders are mainly applied in mini and micro ORC systems. The rotating speed is very high in the single stage radial-inflow turbine, which puts forward strict requirements on bearing, shaft seal and the strength of the rotating parts; this results in higher design and manufacturing cost. On the contrary, the rotating speed of volume type expansion machine is low, usually less than 6000 rpm, involving minor design problems and cost.

The efficiency is quite difficult to compare because of can be very influenced by the operational parameters and its definition can be different in different papers. Turbines tend to have the highest performance, with efficiencies in the order of 70% -85%, but their cost is generally higher.
For what concerns the system operation, sometimes there is the possibility

Table 3.2: Expander resume from Bao and Zhao [10]

| Type | Power [kW] | Speed [rpm] | Cost | Advantages | Disadvantages |
|---|---|---|---|---|---|
| Scroll | 1 - 10 | <6000 | Low | High efficiency, simple manufacturing, light weight, low rotate speed and tolerable two-phase | Low Capacity, lubrication and modification requirement |
| Screw | 15 - 200 | <6000 | Med. | Tolerable two-phase, low rotate speed and high efficiency in off-design conditions | Lubrication requirement, difficult manufacture and seal |
| Turbine | 50-500 | 8000-80000 | High | Light weight, mature manufacturability and high efficiency | High cost, low efficiency in off-design conditions and cannot bear two-phase |

to have liquid at the end of the expansion, which can potentially damage the turbine. The screw and scroll expanders, instead, can tolerate two-phase flows. On the other hand, positive displacement machines have important friction problems; the lubrication of the machine improves the efficiency but requires installing oil separator, increasing the complexity of the system.

The choice between scroll and screw expander often depends on the application. The buil-in pressure ratio is generally higher for screw (up to 5, generally). The scroll expanders show volume ratios ranging from 1.5 to 4. The volume ratio is constrained by performance considerations (limit the friction and leakage losses) and cost considerations (prohibitive unrolled scroll length, compactness). Larger volume ratios could be achieved by associating expanders in series. The power output is generally greater for scroll expanders.

For further information is reported below a recapitulating table 3.2 of advantages and disadvantages of the three technologies analysed.

## 3.3 Models

### 3.3.1 Method of analysis.

This section focuses on the models used to simulate the behaviour of the expander machines. In particular we examine in depth the models for the volumetric expanders because the plant that we aim to simulate is equipped with a double-screw device.

#### Deterministic and empirical approach.

Research on expanders usually involves experimental and theoretical (or deterministic) methods. In the **deterministic approach** a set of equations is established to define the geometry of the expander, including dimensions such as chamber volume and leakage area. Many different mathematical approaches have been developed as [13, 18].
Once the geometry is defined, the working volume is taken as the control volume; for each volume, differential equations of conservation of mass and energy are established and numerically solved. Through energy and mass balance is then possible to calculate all the main performance parameters. The heat losses due to the heat transfer could be described by equations derived from Dittus-Boelter equation.
In the end, a deterministic approach requires a complex mathematical method, which results accurate but also very expensive from a computational point of view.

A completely **empirical method** is based on a "black-box" approach. In fact, the output variables (such as the power generated), are estimated from the measured parameters, using a regression method. A common empirical method is proposed by Avadhanula and Lin [7]. Here the expander power output is estimated using Levenberg–Marquardt regression analysis on two different models: a polytropic and isentropic expansion. The operating parameters used for the fitting are the pressure ratio $r_p$ and volume ratio $r_v$, (defined in eq. 3.1). The specific work output is estimated through the third formula of 3.1. The results obtained are quite good, with a maximum relative error smaller then 10% .

$$r_P = \frac{P_{su}}{P_{ex}} \qquad r_v = \frac{v_{ex}}{v_{su}} \qquad w = \frac{nP_{su}v_{su}}{n-1}(1 - \frac{r_v}{r_p}) \tag{3.1}$$

Empirical models exhibit generally a good precision and are characterized by low computational cost and high numerical robustness. Anyhow they do not allow for extrapolation beyond calibration range.

**Semi-empirical model.**

A third path, which can be very useful in ORC steady-state modelling, is represented by the semi-empirical models. They are based on a limited set of equations representing the main physical processes inherent to the expander models; this theoretical part is then corrected by means of some parameters, connected to a precise physical meaning. Semi-empirical models usually show low computational time and good numerical robustness. They allow for partial extrapolation of the performance.

In order to understand the physical meaning of the parameters used in the following models, we give some hints of the expander real behaviour. We can distinguish these main non-ideality factors:

**Over-expansion and under-expansion:** this event occurs when the internal pressure ratio, imposed by the scroll, is different from the one of the system, so the pressure in the chamber at the end of the expansion is different from the pressure in the discharge line. If the pressure is too high (under-expansion, see figure 3.4b) not all the expansion work is used, if the pressure is lower (over-expansion, figure 3.4b), a certain loss will be caused by the backflow and recompression of the working fluid;

**Internal leakage:** A certain quantity of working fluid flows from high-pressure chambers to low-pressure ones. Inside the expander there are different leakage paths due to the gaps between the plates and the moving parts. Not only leakage area is important in leakage mass flow but also rotational speed and lubrication have great effect.

**Section pressure loss:** Entering the expansion chamber the fluid encounters some pressure losses due to the throttling action of the orifice;

**Heat losses:** The entire expansion process is obviously non-adiabatic.

### 3.3.2 Simple model.

An interesting yet simple model have been proposed by Quoilin et al. [52]. This method has been also used by other authors, such as Hsu et al. [31]. We decided to start the expander modelling from this method, since it has been proven as a simple and effective approach.

The over and under-expansion losses are taken into account considering the real expansion as divided in two fictitious steps:

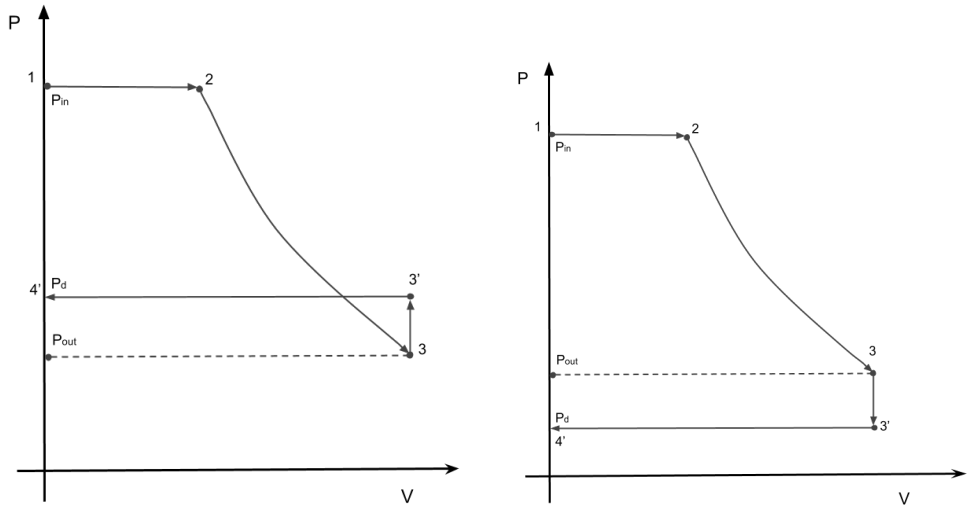


(a) (b)

Figure 3.4: Over- and under-expansion in P-v diagram [40]

1. An isentropic expansion, where the specific work produced can be expressed as

$$w_1 = h_{su} - h_{is}. \tag{3.2}$$

Where $h_{su}$ is the specific enthalpy of the supply stream and $h_{is}$ is the isentropic enthalpy at pressure $P_{int}$, the pressure in the expansion chambers at the end of the expansion process.

2. A constant-volume expansion. The specific work is

$$w_2 = v_{int}(P_{int} - P_{ex}) \tag{3.3}$$

$v_{int}$ is the specific volume at $P_{int}$, $P_{ex}$ is the exhaust pressure. The constant-volume-expansion work ($w_2$) is positive in the under-expansion mode but negative in the over-expansion.

The total expansion work is then obtained by summing $w_1$ and $w_2$. Other losses such as internal leakage, supply pressure drop, heat transfers and friction are lumped into one single mechanical efficiency, so that:

$$W_{exp} = \dot{M}(w_1 + w_2)\ \eta_{mecc} \tag{3.4}$$

The expander mass flow rate depends on rotational speed $N_{rot}$, expander swept volume $V_s$ and supply density $\rho_{su}$:

$$\dot{M} = \frac{\rho_{su} V_s N_{rot}}{60}. \tag{3.5}$$

### 3.3.3 Complete Model

In the second stage of expander study we decided to develop a more complete model, based on the semi-empirical method proposed by Declaye et al. [19]. To obtain a generic non-dimensional performance curve of the expander, a fitted expression of the efficiency can be defined using carefully selected input variables. Unlike the aforementioned article, we also tried to include the heat losses, through a second fitting. The expander isentropic efficiency is defined as:

$$\varepsilon_s = \frac{\dot{W}}{\dot{M}(h_{su} - h_{ex,s})} = \frac{\dot{M}(h_{su} - h_{ex}) - \dot{Q}_{amb}}{\dot{M}(h_{su} - h_{ex,s})}. \tag{3.6}$$

The working conditions used for the fitting are defined by: the inlet pressure $\rho_{su}$, the rotational speed $N_{rot}$ and the pressure ratio over the expander $r_p$. They turned out to be the main representative variables of the working conditions, according to the studies found in literature [19, 52].
The expression chosen is inspired by Pacejka's equation (Pacejka [48]) and is created to present the same shape of the efficiency vs. pressure ratio plot (cfr. 3.5b ).

The efficiency is a function of the three main variables ($\rho_{su}$, $r_p$, $N_{rot}$) and five coefficients ($y_{max}$, $r_{p,0}$, $r_{p,max}$, $\xi$, $\delta$) :

$$\varepsilon_s = y_{max}\ \sin\left\{\xi\ \arctan\left[B(r_p - r_{p,0}) - E\Big(B(r_p - r_{p,0}) - \arctan\big(B(r_p - r_{p,0})\big)\Big)\ \right]\right\} \tag{3.7}$$

Where:

$$B = \frac{\delta}{\xi y_{max}}; \qquad E = \frac{B(r_{p,max} - r_{p,0}) - \tan(\frac{\pi}{2\xi})}{B(r_{p,max} - r_{p,0}) - \arctan(B(r_{p,max} - r_{p,0}))}$$

Since the efficiency varies with the pressure and rotating speed, the parameters are expressed as a function of the non-dimensional working conditions, represented in 3.8. The nominal values used for pressure ratio, rotational speed and pressure are respectively: 4, 5000 *rpm* and 10 *bar*.

$$\hat{r_p} = \frac{r_p - r_{p,nom}}{r_{p,nom}}; \quad \hat{N}_{rot} = \frac{N_{rot} - N_{rot,nom}}{N_{rot,nom}}; \quad \hat{P} = \frac{P - P_{nom}}{P_{nom}}. \tag{3.8}$$

The parameters are then expressed as a linear regression using the empirical coefficients $a_x$, $r_{p,0,n}$, $\delta_n$, $\xi$, $r_{p,max,n}$, $N_{rot,n}$, $y_{max,n}$ :

$$r_{p,0} = r_{p,0,n} + a_0 \hat{N}_{rot} \ ; \tag{3.9}$$

$$\delta = \delta_n + a_1 \hat{P} + a_2 \hat{N}_{rot} \ ; \tag{3.10}$$

$$r_{p,max} = r_{p,max,n} + a_3 \hat{P} + a_4 \hat{N}_{rot} \ ; \tag{3.11}$$

$$y_{max} = y_{max,n} + a_5 \hat{P} + a_6 (\hat{N}_{rot} - \hat{N}_{rot,n})^2 \ . \tag{3.12}$$

Volumetric performance of the machine was quantified through the **filling factor** $\phi$, defined as the ratio of the measured mass flowrate and the mass flowrate theoretically displaced by the expander:

$$\phi = \frac{\dot{M} v_{su}}{V_s}.$$

The filling factor is expressed in this model as a linear regression of the non-dimensional parameters through the following relation:

$$\phi = \phi_n + b_0 \ \ln(\frac{N_{rot}}{N_{rot,nom}}) + b_1 \ \hat{r_p} + b_2 \ \hat{P}$$

$\phi_n$ and $b_x$ are the coefficients that have to be found in the fitting.

The path that we followed to find all the coefficients is resumed below:

1. Using the aforementioned operating parameters we calculate the expander efficiency and the exhaust enthalpy;

2. We calculate the filling factor and thus the mass flow rate;

3. The shaft power is obtained through the mass flow rate and the enthalpy difference;

4. The generator efficiency is calculated. This is composed by the generator efficiency, set to 0.98, and by the inverter efficiency, expressed by a correlation given by the manufacturer;

5. The electrical power is finally obtained multiplying the shaft power by the generator efficiency. The optimizer compares this value to the empirical power and iterates to find the coefficients.

Now that the shaft power is known, a new fitting is run in order to find the heat losses. The exhaust enthalpy is finally calculated using the formula 3.6.

## 3.4 Results and validation of the model.

### 3.4.1 Expander performance

In this section we briefly present the results obtain for the expander performance. This is evaluated in terms of isentropic efficiency and electrical power generated, for different values of pressure ratio and supply pressure. In fact the first aim is to compare our results with the conclusions of other articles.

For our test campaign we can distinguish 13 different points, subdivided in 3 groups, depending on the supply pressure: 9.5, 11.5 and 12.5 bar. The pressure ratio varies between 3.9 and 5, while the expander rotational speed is fixed at 5000 *rpm*
The measured electrical power output $W_e$ is shown in Figure 3.5a, as a function of applied pressure ratio for three different inlet pressures. It can be observed that the shaft power is an increasing function of the pressure ratio; for a given speed, a higher inlet pressure yields more power. This happens because the density is higher at higher pressure, hence the swept mass flow rate in the expander is higher. The maximum power is about 6.45 kW for a pressure ratio of 4.9 and an inlet pressure of 12.5 bar. The minimum power is 4.11 kW for a pressure ratio of 4.1 and an inlet pressure of 9.5 bar.

The expander isentropic efficiency $\varepsilon_s$ is represented in Figure **??** as a function of $r_p$ and appears to be an increasing function of the pressure ratio in this area. In fact, as observed by [41], the efficiency significantly increases with $r_p$, for pressure ratios smaller then the built-in volumetric ratio. Moreover, the maximum efficiency is reached around the build-in ratio, since the over and under-expansion losses are minimized; the value of the pressure ratio that maximizes the isentropic efficiency is not constant due to other additional influences such as leakages, friction losses, etc. .
Since the rotational speed is always constant and the inlet pressure values are quite similar, the efficiency doesn't show relevant variations. The maximum value is around 60 % for a pressure ratio of $4.9 - 5$, close to the built-in value.

In Figure 3.6 the mass flow rate is represented as a function of the inlet pressure. The mass flow value is obviously an increasing function of the inlet density, which directly depends on inlet pressure and temperature. In particular, the influence of pressure is evident, while the temperature difference for a given pressure only generates a little spread.

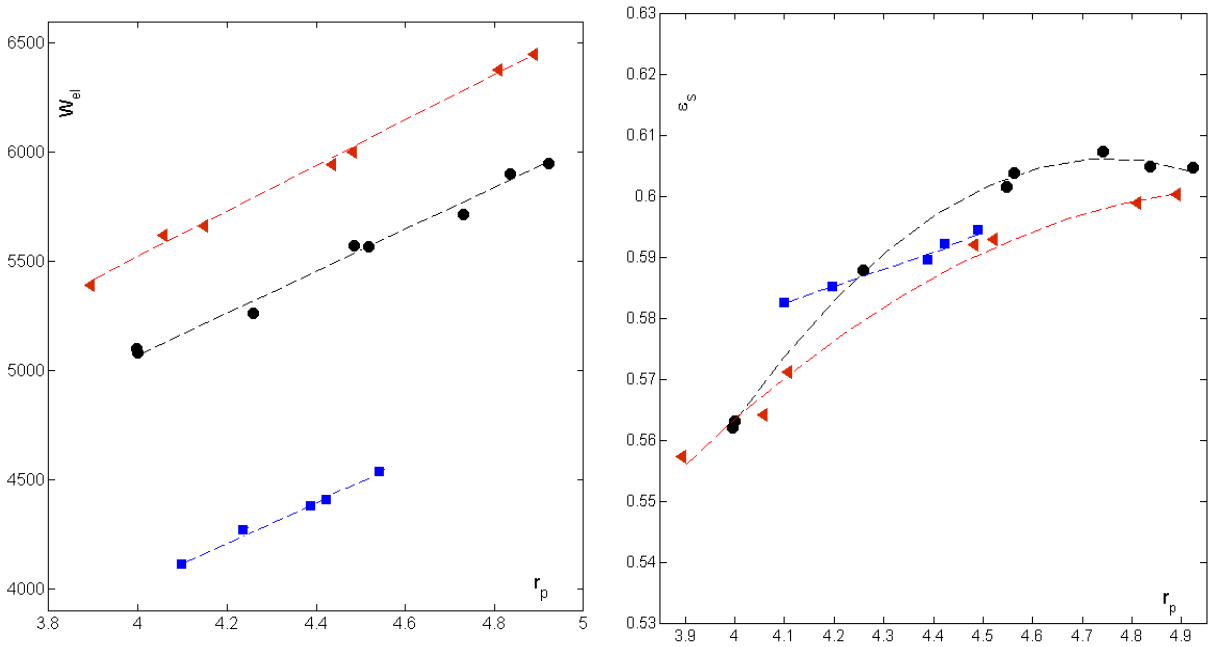


(a) Shaft power as a function of $r_p$ (b) Expander efficiency as a function of $r_p$

Figure 3.5: Shaft power and expander efficiency for 3 different pressures.

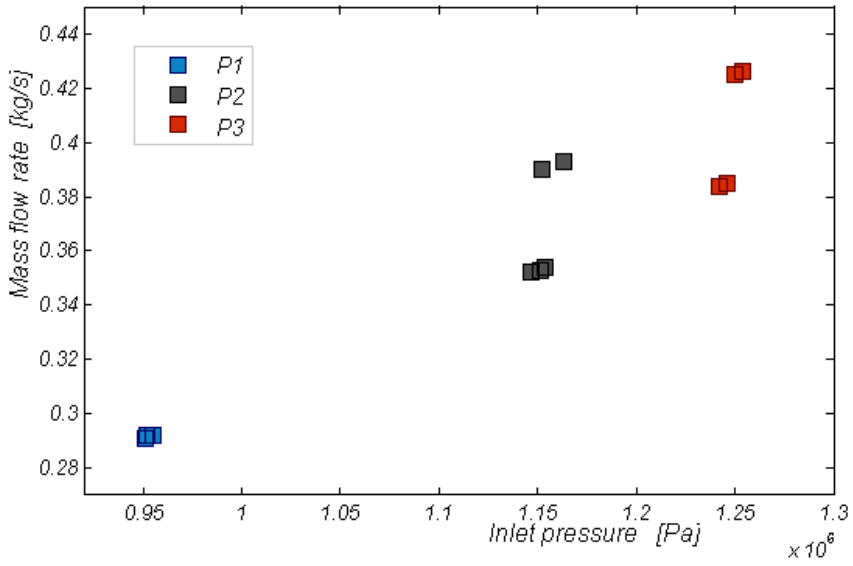


Figure 3.6: Expander mass flow rate as a function of inlet pressure.

### 3.4.2 Validation of the model.

In the following section are represented the results obtained with the simple and complete model, introduced above. In order to compare the results obtained to the experimental data a parity plot for exhaust enthalpy and mass flow rate are represented in Figure 3.7a and 3.7b respectively. The y=x line is also plotted as a reference. Moreover two parameters are used to evaluate the goodness of each model: the *Relative Error, RE* and *mape (mean absolute percentage error)* defined as follows:

$$RE = \left| \frac{y - \hat{y}}{\hat{y}} \right| \qquad mape = \frac{1}{n} \sum_{k=1}^{n} \left| \frac{y - \hat{y}}{\hat{y}} \right|$$

For what concerns the exhaust enthalpy we can see that the complete model shows better results, compared to the simple model. The maximum relative error obtained is 2.48% for the simple model and 0.52% for the complete one. The *mape* values are 1.51% and 0.26% respectively. The values obtained from the complete model are thus more precise, even if the error coming from the base model was quite good.
The mass flow rate values obtained from the two models are quite close, with no particular improvement due to the fitting. In fact, the maximum relative error obtained for the simple model is 4.64 % and 3.11% for the complete one.

In the end, comparing enthalpy and mass flow rate the fitted model of the expander shows better results compared to the basic one but the difference is not so big. That is probably due to the easy and steady state conditions that we have chosen. In fact, in this case was rather easy to set a value of efficiency to adequately fit the exhaust enthalpy. Moreover the expander rotational speed, which is the most important variable for the mass flow rate, is fixed; so it appears reasonable that even the simple model provides good results. However, the precision of the model becomes far more important if we refer to the expander power. In fact, the values of power coming from the simple model are not satisfactory at all and the maximum relative error is higher then 20%. The propagation of error and the influence of other factors (such as generator efficiency) become influential in the calculation of this variable.

For this reason we decided to fit the model on the expander power and then add another polynomial fit for the heat losses. The fitting used in the optimizer is a polynomial function of expander rotational speed, inlet pressure and enthalpy. The results obtained are not very good, with a maximum relative error of 9.3 % but this choice is justified by the good precision on

enthalpy and output power. The values of power obtained from the simulation are reported in Figure 3.8. This plot shows the value of power as a function of pressure ratio at different inlet pressures. The lines are the results of the model while the dots represent the experimental data. The maximum relative error obtained is 4.30% and the *mape* value is 0.44%.

### 3.4.3 Conclusions.

From the analysis of the models and the simulation results, we can infer the following conclusions:

- The simple model proposed can give satisfactory results in the analysis of the exhaust enthalpy and mass flow rate. This is possible however, only for a steady-state condition and constant expander speed; moreover the expander technical parameters need to be known and also an hint of the expander efficiency value is required.
- The complete model is obtained fitting the coefficients on the shaft power. That implies a good result on enthalpy and power error but slightly penalize the efficiency and heat losses precision. This choice was driven by the need to implement this simulation tool inside a bigger model for the entire ORC; the enthalpy and power are, in deed, the most important variables in this viewpoint.
- The complete model built can be a simple and precise tool to simulate the expander behaviour and can be easily included in another system simulation.

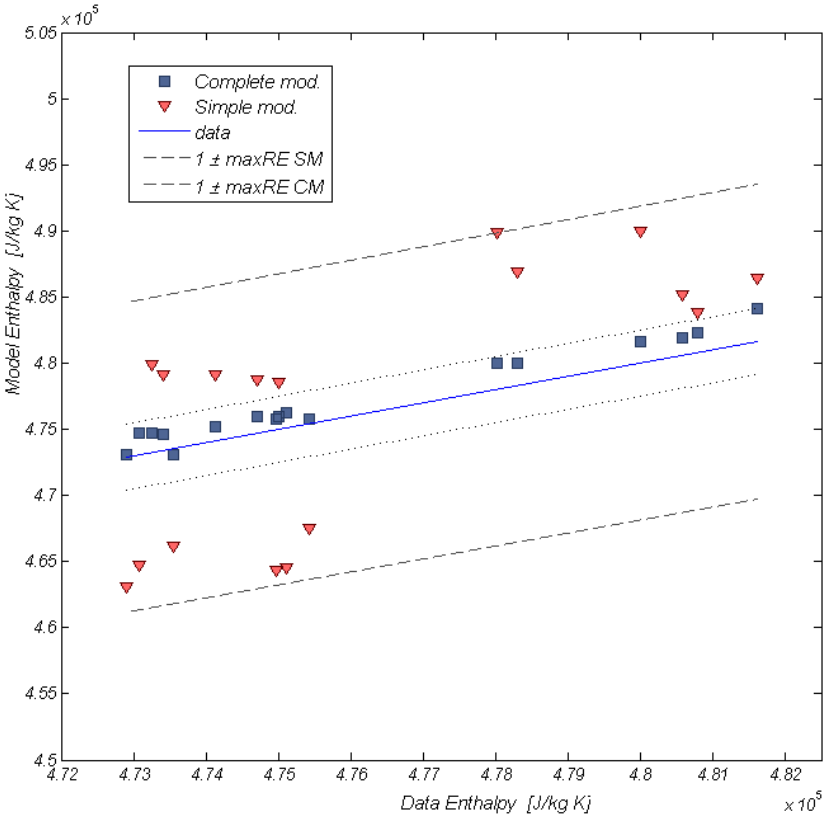


(a)

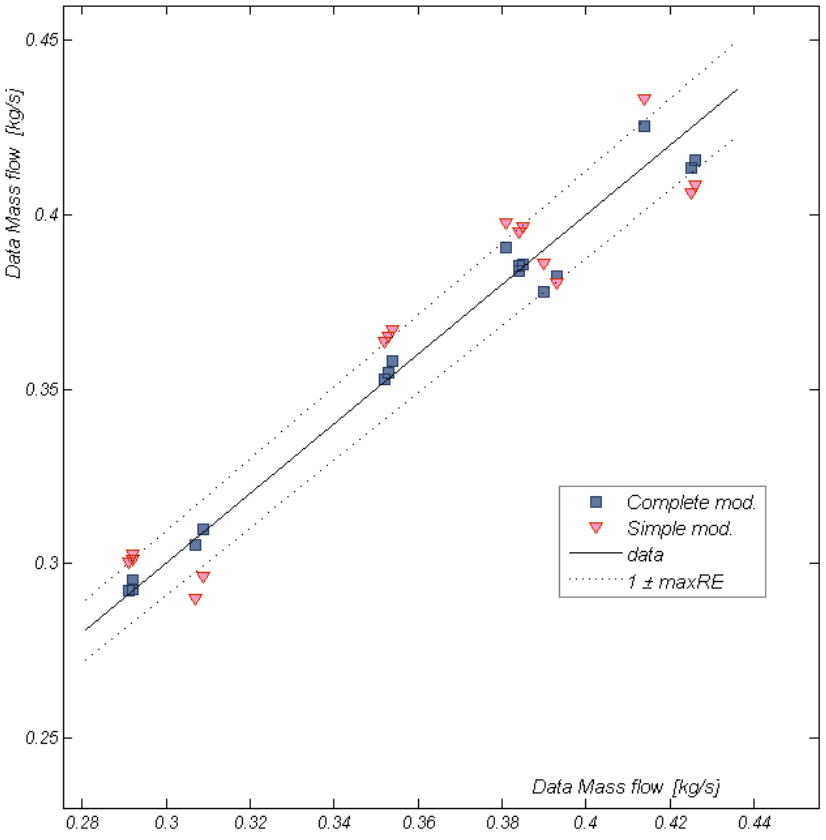


(b)

Figure 3.7: Results for exhaust enthalpy and mass flow rate using the simple and complete model.

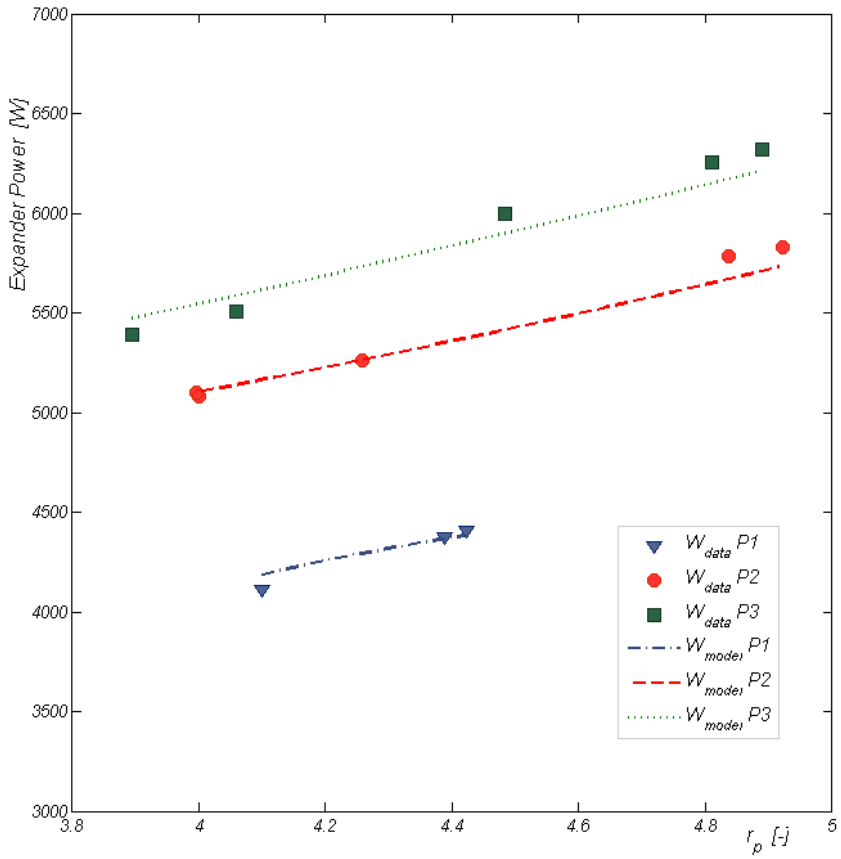


Figure 3.8: Expander power as a function of pressure ratio, model and experimental data.

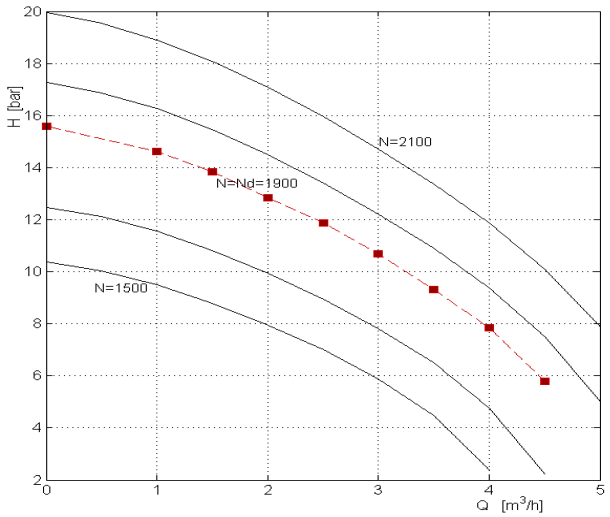


Figure 3.9: Pump characteristic.

## 3.5 Pump model

A brief description of the pump modelling approach is reported in this section. The simulation of this element was not considered crucial for the development of this study and its description will be very quick.
In fact, studying and developing a model for the expander is very important in the ORC simulation because this element is in constant development; moreover almost every company has developed its own technology. The pump, instead, is a standard element in many different systems and, usually, it is not subjected to any particular modification or development.
As a result, the standard pump characteristic curve provided by the manufacturer is a sufficient tool to describe the pump performance.

In the ORC modelled here, a centrifugal pump with variable frequency drive is used. Given the pump model it was easy to find the manufacturer curve and implement it in a *matlab* function. Since the curve is given just for a particular rotational speed (the nominal value) it was necessary to adopt the *affinity laws*.
The affinity laws allow prediction of the head discharge characteristic of a pump or fan from a known characteristic measured at a different speed or impeller diameter. The only requirement is that the two pumps or fans are geometrically similar and operated at dynamically similar conditions or equal specific speed. These laws assume that the pump efficiency remains constant, which is rarely exactly true, but can be a good approximation in many applications.

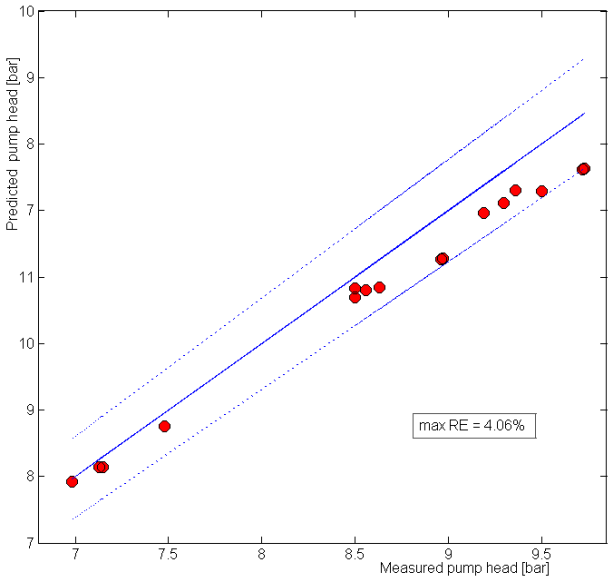


Figure 3.10: Pump Head, parity plot.

The use of this assumption is very common in the pump simulation and can be expressed as follows:

$$\frac{Q_1}{Q_2} = \frac{N_1}{N_2} \qquad \frac{H_1}{H_2} = \left(\frac{N_1}{N_2}\right)^2 \qquad \frac{P_1}{P_2} = \left(\frac{N_1}{N_2}\right)^3$$

In these formulas $Q$ is the volumetric flow rate, $H$ is the pump head, $P$ is the absorbed power and $N$ is the pump rotational speed. The subscripts 1 and 2 indicate two different working points. Using these equations it is possible to determine any other working point as a comparison to the nominal conditions. In figure 3.9 the resulting performance curves are drawn for nominal speed as well as for different speeds.

The pump characteristic curves and the affinity laws have been used to create a model of the pump. This model connects the mass flow rate, to pump head and absorbed power. The results obtained have been compared to the experimental data, obtaining a good agreement between the model and the measured data.
A parity-plot representing the predicted and measured pump head have been represented in figure 3.10. The maximum relative error obtained for the pump head is 4.06%, while the power predicted presents a maximum relative error of 6.72%.

# Chapter 4

# Heat exchangers analysis and simulation.

## 4.1 Introduction.

Together with the expander, the heat exchangers are the most important elements for the simulation of an ORC system. In fact, the heat exchanger design deeply influences the overall efficiency and performance.
In this section the main models to simulate an heat exchanger will be analysed and compared. In particular we are interested in the steady-state behaviour so the traditional models will be analysed. Some hints are given also on pressure drop and heat transfer, for the sake of completeness.

## 4.2 Heat exchangers models.

For a sizing problem, where one must define the required area of a heat exchanger in order to achieve the desired outlet temperatures and/or heat transfer rate $q$, the main parts of the problem can be said to consist of two parts:

1. finding the value of overall heat transfer coefficient U for the type of heat exchanger at hand;

2. finding the correct way to get to the required heat transfer area given the U value, selected type of heat exchanger and fluid conditions.

The first part of the problem is mainly an issue of estimating the correct convection heat transfer coefficients at the heat transfer surface. Determining

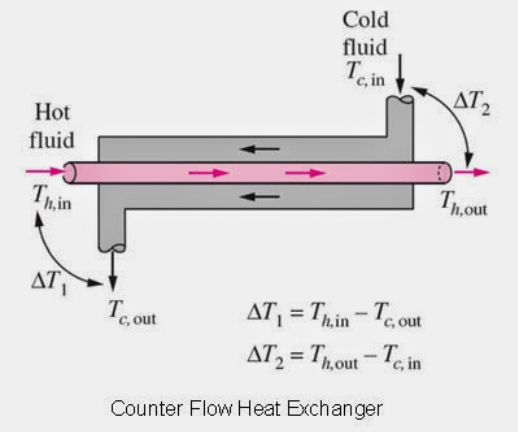


Figure 4.1: Counter-flow heat exchanger scheme.

the value of U is thus mainly a function of the exact physical geometries and flow characteristics.

Various heat exchanger sizing methods have been developed from the basic transfer rate and conservation equations, each giving different methods to relate the overall heat transfer coefficient U and fluid temperatures and heat capacity rates $C$ to the required heat transfer area. All these methods are based on certain simplifying assumptions:

- There is no heat transfer between the fluid streams and the outside environment. No heat is generated or lost trough other means.
- There is no heat conduction along the length of the heat transfer surface, only in the direction of the normal of the surface
- The model based on a steady-state concept, and cannot be used in dynamic analyses.

The architecture considered in Figure 4.1 is the most simple one: a double pipe heat exchanger. However the model obtained can be easily applied to different types of devices.

### 4.2.1 Logarithmic mean temperature difference LMTD.

Let the pipes length be of equal to $L$, carrying fluids with heat capacity $c_i$ (energy per unit mass per unit change in temperature) and let the mass flow rate of the fluids through the pipes be $m_i$ (mass per unit time), where the subscript $i$ applies to pipe 1 or pipe 2. The temperature profiles for the pipes are $T1(x)$ and $T2(x)$, where x is the distance along the pipe. Assume

a steady state so that the temperature profiles are not functions of time and that there is no transfer of heat along a pipe due to temperature differences in that pipe.

The two fluids are separated by an interface of area $A$ and the heat transfer is due to the convection between fluid and wall, represented by the *overall heat transfer coefficient* $U$. This parameter takes into account the individual heat transfer coefficients of each stream and the resistance of the pipe material ; the calculation of this parameter will be discussed in section 4.2.4 on page 52.

The overall heat exchanged can be derived integrating the heat through the infinitesimal area $dA$, between inlet and outlet sections:

$$d\dot{Q} = -\dot{m}_1 c_{p,1} dT_1 = \dot{m}_2 c_{p,2} dT_2 d\dot{Q} = U dA(T_1 - T_2).$$

Obtaining:

$$d\dot{Q} = UA\frac{\Delta T_1 - \Delta T_2}{\ln \frac{\Delta T_1}{\Delta T_2}} = UA\Delta T_{LMTD}.$$

Where $\Delta T_1$ is the temperature difference at the inlet section and $\Delta T_2$ at the outlet section.

$$\Delta T_1 = T_{1,in} - T_{2,out} \qquad \Delta T_2 = T_{1,out} - T_{2,in}$$

This derivation holds both for co-current flow, where the streams enter from the same end, and for counter-current flow, where they enter from different ends. For other different types of exchangers a correction factor should be applied; the correction factor depends on the temperatures and type of heat exchanger and is usually given by the manufacturer.

LMTD method is usually applied to design an heat exchanger under prescribed temperatures and mass flow rate. The inlet and outlet temperatures of the hot and cold fluids are usually specified in this analysis. The goal of the LMTD method is thus to select a heat exchanger that will meet the prescribed heat transfer requirements.

### 4.2.2 Effectiveness - NTU method

Another possible approach in heat exchanger analysis is the determination of the heat transfer rate and the outlet temperatures for prescribed mass flow rates and inlet temperatures. The heat exchanger type and geometry are specified; the goal is to determine the heat transfer performance. In this case, the effectiveness–NTU method could be more suitable.

The $\varepsilon - NTU$ method is based on three dimensionless parameters: the heat exchanger *effectiveness* $\varepsilon$, the *heat capacity ratio* $C_r$ and the number of transfer units $NTU$.

The parameter $C_r$ is the ratio of the heat capacity rates of the fluid streams, defined as the ratio of smaller to the larger.

$$C_r = \frac{C_{min}}{C_{max}} = \frac{(q_m c_p)_{min}}{(q_m c_p)_{max}}$$

If one of the fluids of the heat exchanger experience a phase change, then the temperature of that fluid stream does not change, and $C$ of that stream is effectively infinity and the heat capacity rate ratio will be 0.

The NTU parameter is the one which contains the independent design variable under the heat exchanger designer's control: overall heat transfer rate U and heat transfer surface area A. NTU is defined as:

$$NTU = \frac{UA}{C_{min}}$$

The *effectiveness* is defined as the ratio between the actual heat transfer rate and the maximum possible heat transfer rate:

$$\varepsilon = \dot{Q}/\dot{Q}_{max}.$$

The maximum heat transfer in a counterflow heat exchanger could be reached when the minimum heat capacity rate fluid has experienced the entire temperature change $T_{h,i} - T_{c,i}$; where $T_{h,i}$ is the hot fluid inlet temperature and $T_{c,i}$ the cold inlet temperature. This limiting condition can only appear in a infinite area heat exchanger. The heat rate of the real exchanger can be expressed as:

$$\dot{Q} = \varepsilon C_{min}(T_{h,i} - T_{c,i})$$

Functions correlating the three dimensionless parameters to each other exist for a variety of flow arrangements. Effectiveness-NTU relationships are tabulated in both equation and graphical form in numerous heat transfer textbooks and heat exchanger design handbooks. An example of a graphical correlation for $\varepsilon$ is shown in Figure 4.2.

### 4.2.3 P-NTU method.

Sometimes, can be useful to use a different parameter instead of $\varepsilon$ to avoid possible errors and confusion in computer modelling of particular heat exchangers. An alternative to effectiveness is to present the *temperature effectiveness* $P$ for every fluid stream:

$$q = P_1 C_1 \Delta T_{max} = P_2 C_2 \Delta T_{max}.$$

$C_{1,2}$ are the heat capacity rates for fluid 1 or 2 and the inlet temperature difference is $\Delta T_{max} = T_{h,1} - T_{c,i} = |T_{2,i} - T_{1,i}|$. We use the general subscripts 1 and 2 in the $P - NTU$ method with no distinction needed for $C_{max/min}$ or hot and cold fluid.
The temperature effectiveness is non-dimensional and for each stream, $P$ is a function of $NTU$ (based on that side's heat capacity rate) and a ratio of heat capacity rates of that side to the other side, $R$. $R$ can vary from 0 to 1, and only one $P$-$NTU$ formula will sufficient for the complete operating range of the exchanger. The parameters are defined as follows:

$$P_1 = \frac{T_{1,o} - T_{1,i}}{T_{2,i} - T_{1,i}}; \quad P_2 = P_1 R_1; \tag{4.1}$$

$$NTU_1 = \frac{UA}{C_1} \quad NTU_2 = NTU_1 R_1; \tag{4.2}$$

$$R_1 = \frac{C_1}{C_2} = \frac{T_{2,i} - T_{2,o}}{T_{1,o} - T_{1,i}} \quad R_2 = 1/R_1; \tag{4.3}$$

The equation that connects P to NTU and C depends on the flow arrangement. The formulas for many different flow arrangements can be found in [56].

The equation 4.4 represents the $P$ correlation for a 1 pass–1 pass counterflow plate exchanger, as the one used in the selected power plant.

$$P = \frac{1 - e^{-NTU(1-C)}}{1 - Ce^{-NTU(1-C)}} \tag{4.4}$$

### 4.2.4 Heat transfer correlations.

The calculation of the overall heat transfer coefficient is at the basis of the heat exchanger design problem. It can be calculated as the reciprocal of the sum of a series of thermal resistances using the analogy between thermal and electrical circuits:

$$\frac{1}{UA} = \frac{1}{h_1 A_1} + R_p + \frac{1}{h_2 A_2}$$

where $h_1$ and $h_2$ are the heat transfer coefficients of the two sides of the heat exchanging surface. $R_p$ is the thermal resistance of the wall and is generally very small compared to the other terms.

Determining the convection heat transfer coefficient $h$ is the step that typically produces the greatest inaccuracies in heat exchanger analysis. This is because exact analytical solutions are available only for laminar flow situations, and in actual heat exchangers the flow is almost always turbulent.

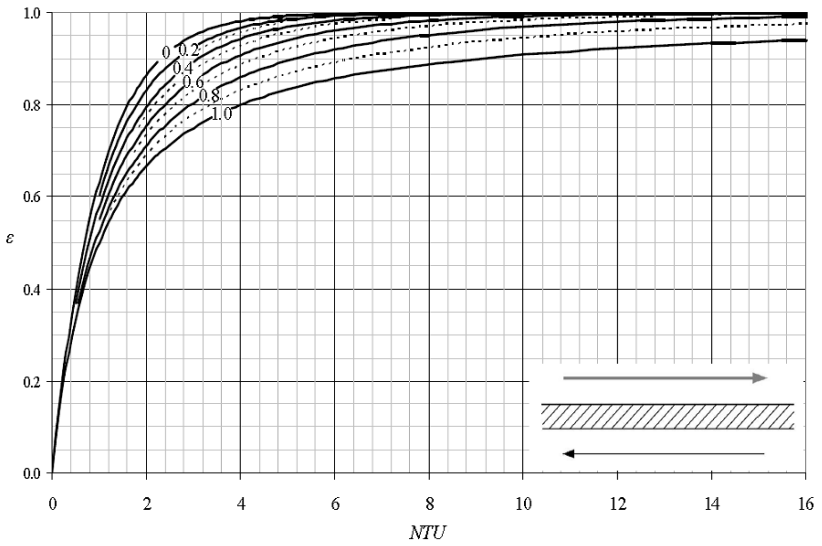


Figure 4.2: Counter-flow $\varepsilon - NTU correlation$.

Therefore the convection heat transfer coefficient must be obtained from empirical correlations, which frequently have margins of error of 10 to 30%. The empirical correlations are expressed as a function of some empirical constants and dimensionless parameters; they have a different form for single-phase and two-phase flows.

The dimensionless parameters used are the usual ones of thermo-fluid dynamics:

- *Reynolds number:*
$$Re = \frac{uD_h\rho}{\mu} = \frac{D_hG}{\mu}.$$
where $u$ is the velocity, $\rho$ and $\mu$ are the fluid density and dynamic viscosity and $D_h$ is the hydraulic diameter, a characteristic length depending on the geometry. Is usually convenient to express the Reynolds number in terms of *mass velocity* $G = u\rho = \dot{m}A_p$, where $A_p$ is the passage area for the mass flow $\dot{m}$.

- *Nusselt number:* Is the central parameter in convection and allows to calculate the heat transfer coefficient $h$:
$$Nu = \frac{hD_h}{k_f}.$$
where $k_f$ is the thermal conductivity of the fluid.

- *Prandtl number:*

$$Pr = \frac{\mu c_p}{k_f}$$

- *Boiling number*: used in two-phase analysis, represents the ratio of the actual heat flux to the maximum heat flux achievable by complete evaporation of the liquid.

$$Bo = \frac{\dot{q}}{h_{lat}\dot{m}}$$

  In this formula $\dot{q}$ is the heat flux per unit area and $h_{lat}$ is the latent heat of vaporization.

**Single-phase flow**

A lot of correlations have been proposed for single-phase conditions and they are usually presented in the following form:

$$Nu = CRe^m Pr^n$$

In this equation $C$, $m$ and $n$ are constants, chosen according to various experimental optimizations.
Each correlation has its own range of applicability and is more suitable for a particular condition and fluid.

In this work we have test different correlations in order to obtain the best accuracy. The correlation used is the one proposed by Martin [45]. His study is conducted on chevron-type plate heat exchangers and derives a relatively simple but physically reasonable equation for the friction factor $\xi$ as a function of the chevron angle $\beta$ and the Reynolds number $Re$. The heat-transfer coefficients are obtained from a theoretical equation for developing thermal boundary layers in fully developed laminar or turbulent channel flow. This prediction is in good agreement with our experimental observations.
The equation used for the Nusselt number is:

$$Nu = c_1 Pr^{1/3}(\eta/\eta_w)^{1/6}[\xi Re^2\ sin(2\beta)]^{c_2}.$$

$c_1$ and $c_2$ are the empirical constants while $\xi$ is the friction factor. The latter is calculated with a different expression depending on the flow regime:

$$\frac{1}{\sqrt{\xi}} = \frac{cos\beta}{\sqrt{0.18\ tan\beta + 0.36\ sin\beta + \xi_0/cos\beta}} + \frac{1 - cos\beta}{\sqrt{\xi_1}}.$$

$$\begin{aligned} &\xi_0 = 64/Re && \text{if } Re < 2000 \\ &\xi_1 = 597/Re + 3.85 \end{aligned}$$

$$\begin{aligned} &\xi_0 = 1/(1.8\ \ln Re - 1.5)^2 && \text{if } Re > 2000 \\ &\xi_1 = 39/Re^{0.289} \end{aligned}$$

During the simulation process the coefficients $c_1$ and $c_2$ have been slightly modified, in order to better comply with our experimental results.

**Two-phase flow**

The heat transfer coefficients for evaporation and condensation have been obtained using an expression developed by Han et al. [28, 29]. Their experiments were performed on a brazed plate heat exchanger with the refrigerants R410A and R22. Brazed plate heat exchangers with different chevron angles were used. The dependence of the Nusselt number on the geometrical parameters is expressed though the coefficients $Ge_1$ and $Ge_2$.

For evaporation:

$$\begin{aligned} Nu &= Ge_1\ {Re_{eq}}^{Ge_2}\ {Bo_{eq}}^{0.3}\ Pr^{0.4} \\ Ge_1 &= 2.81\ (\frac{p_{co}}{D_h})^{-0.041}\ (\frac{\pi}{2} - \beta)^{-2.83} \\ Ge_2 &= 0.746\ (\frac{p_{co}}{D_h})^{-0.082}\ (\frac{\pi}{2} - \beta)^{0.61} \end{aligned}$$

the subscript $eq$ indicates that the Reynolds and Boiling number are calculated using the equivalent mass flux: $G_{eq} = G[1 - x + x(\rho_f/\rho_g)^{1/2}]$. In this expression $G$ is the single-phase mass flux, $x$ is the quality of vapour and the densities are referred to gas and liquid. The expression of Nusselt for condensation instead, doesn't contain the boiling number:

$$\begin{aligned} Nu &= Ge_1\ {Re_{eq}}^{Ge_2}\ Pr^{1/3} \\ Ge_1 &= 11.22\ (\frac{p_{co}}{D_h})^{-2.83}\ (\frac{\pi}{2} - \beta)^{-4.5} \\ Ge_2 &= 0.35\ (\frac{p_{co}}{D_h})^{-0.23}\ (\frac{\pi}{2} - \beta)^{1.48} \end{aligned}$$

In order to obtain a better precision, both evaporating and condensing Nusselt numbers have been slightly corrected, using a empirical multiplying coefficient.

## 4.3 Heat exchanger simulation.

Using the correlations and models explained in the previous section we built a model for evaporator and condenser. For every heat exchanger a model have been built and tested. In fact, for every test condition, the results coming from the model have been compared to the data measured on the power plant.

The model that we decided to build receives as inputs the outlet temperature of the working fluid and the inlet temperature of the secondary fluid and calculates the temperatures on the other side: working fluid inlet and secondary fluid outlet. The mass flow rate is given for both the fluids, as well as the pressure. Moreover, the geometric data of the heat exchanger are known so the total heat exchanging area ($A_exch$) can be calculated. The inputs and outputs of the model are resumed in Table 4.1. The procedure to test the model was the following:

1. A set of test conditions for the inputs variables have been extrapolated from the experimental data;
2. The inputs variables have been used as inputs for the model of the heat exchanger and the output variables have been calculated;
3. The results of the model are compared to the experimental data.

The focus of our study was the steady state behaviour and the relation between power input and power output. That is the reason why the pressure drops and the dynamic phenomena have been neglected.

Table 4.1: Inputs and outputs of the heat exchanger model.

| **Inputs** | **Outputs** |
|---|---|
| $T_{wf,OUT}$, $T_{sf,IN}$ | $T_{wf,IN}$, $T_{sf,OUT}$ |
| $\dot{m}_{wf}$, $\dot{m}_{sf}$ | Q |
| $P_{wf}$, $P_{sf}$ | |
| $A_{exch}$ | |

### 4.3.1 LMTD model.

A first attempt of building a model was based on the logarithmic mean temperature difference (LMTD) method, following a three-zone approach. This method have been used by many other author as Lecompte et al. [37]. The

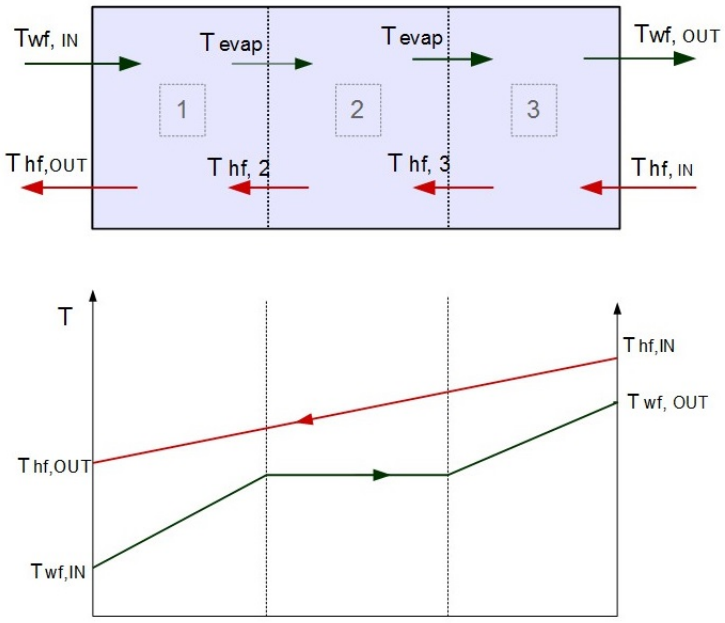


Figure 4.3: Evaporator 3-zones model.

heat exchanger is divided into 3 fictitious zones. If we consider the evaporator model, in the first zone the working fluid is heated to the evaporating temperature; in the second the evaporation takes place and in the third zone the organic compound is super-heated. This concept is represented in Figure 4.3; The upper figure, in particular, represents the three zones of the heat exchanger, while the lower figure represents the qualitative temperature evolution.
In the same way the three zones of the condenser correspond to: cooling of the gas to the condensing temperature, condensation until saturated liquid and, finally, sub-cooling.
It can be important to underline that the overall heat transfer coefficients, U, are different for every section. Moreover, the heat transfer area of each section must be evaluated.

From now on we will describe the mathematical problem only for the evaporator but the considerations are obviously analogous for the condenser. We decide to call $T_{hf,2}$ and $T_{hf,3}$ the temperature of the heating fluid at the beginning of zone 2 and 3. Since the pressure of the working fluid is given, we can use the thermodynamic library to find: $T_{evap}$, $h_{sl}$ and $h_{sv}$. The heat transfer coefficients are calculated using the correlations of the previous section (4.2.4) and the mass flow rates.

Applying the LMTD method for each section we obtain a system of 7 equations for the 7 unknown variables: $T_{wf,in}$, $T_{hf,2}$, $T_{hf,3}$, $T_{hf,out}$, $A_{1,2,3}$.

$$\begin{cases} Q1 = \dot{m}_{wf}\ (h_{sl} - h_{wf,in}) = \dot{m}_{hf}\ (h_{hf,2} - h_{hf,out}); \\ Q1 = U_1\ A_1\ LMTD_1(T_{wf,in}, T_{evap}, T_{hf,3}, T_{hf,out}); \\ \\ Q2 = \dot{m}_{wf}\ (h_{sv} - h_{sl}) = \dot{m}_{hf}\ (h_{hf,3} - h_{hf,2}); \\ Q2 = U_2\ A_2\ LMTD_2(T_{evap}, T_{hf,2}, T_{hf,3}); \\ \\ Q3 = \dot{m}_{wf}\ (h_{wf,out} - h_{sv}) = \dot{m}_{hf}\ (h_{hf,in} - h_{hf,3}); \\ Q3 = U_3\ A_3\ LMTD_3(T_{wf,out}, T_{evap}, T_{hf,3}, T_{hf,in}). \\ \\ A_1 + A_2 + A_3 = A_{exch}. \end{cases} \tag{4.5}$$

The first *Matlab* model, simulated the heat exchanger by solving this system of equations. In particular, for a given set of inputs (mass flow rates, pressures, $T_{wf,out}$ and $T_{hf,in}$) the solution process was the following:

1. A guess value for the temperature distribution is assumed; these values are used to define a medium temperature for each zone.

2. For every zone, the physical properties of the two fluids are calculated using the medium temperature. An external function uses the correlations to compute the overall heat transfer coefficient. This parameter is strongly influenced by the mean temperature and mass flow rate.

3. The system of equations 4.5 is solved. The values of the variables obtained are used as guess values in a new iteration.

Even if the solution of this problem should always exist, some issues arose in the application of this model. First of all, the model showed some troubles of convergence and stability. In fact, for some particular inputs, the goodness of the guess values had a great influence on the solution. A guess value too far from the real solution easily led to instability. In particular, for a high mass flow rate of the heating fluid, it was very hard to find a good guess value.
Another problem was the precision of the results. In fact, comparing the inlet temperature of the working fluid calculated by the model and the real data from the power plant, the error is too high. In particular the maximum relative error of some points was bigger them 15%, corresponding to more then 20° C of error in the temperature value. This problem of precision

didn't appear in all the points tested and it was not immediately addressable to a specific cause.
Anyway, a particular cause of error can be found in the calculation of the heat transfer coefficients. As we have already said, the coefficient $U$ appeared to be strongly dependant on the mean temperature used to compute the physical properties. That could be a possible cause of instability. In fact, a guess value is needed to initialize the solver; if the guess is not good enough the iteration process could diverge.

In the end, this model was not suitable for our goal. Even if the precision could have been increased, the stability remained a distasteful problem. In fact, the heat exchanger model is supposed to be reliable and easy to use, so that can be included in a complete model of the ORC.
For all these reasons we changed the modelling approach and build another model.

### 4.3.2 Sequential model.

The second modelling approach was based on the $P - NTU$ method and solves the temperature distribution over a bigger number of elements. Again we will explain the algorithm operating principles only for the evaporator. The application to the condenser is completely similar.

The conceptual scheme of this model is represented in Figure 4.4. The heat exchanger is divided into **n** elements (with $n > 10$). The algorithm solves sequentially the temperature distribution of the fluids starting from the first element on the right. In this section the temperatures on the right are given ($T_{wf,out}$ and $T_{hf,in}$) while the temperatures on the left need to be evaluated ($T_{wf,1}$ and $T_{hf,1}$). In order to find the 2 unknown variables, the $P - NTU$ method is applied.
Now the solver can be applied to the next element and so on, until the temperatures on the left side of the evaporator are obtained ( $T_{wf,in}$ and $T_{hf,out}$). For every element the overall heat transfer coefficient ($U_j$) need to be calculated using a mean temperature, while the area is given.

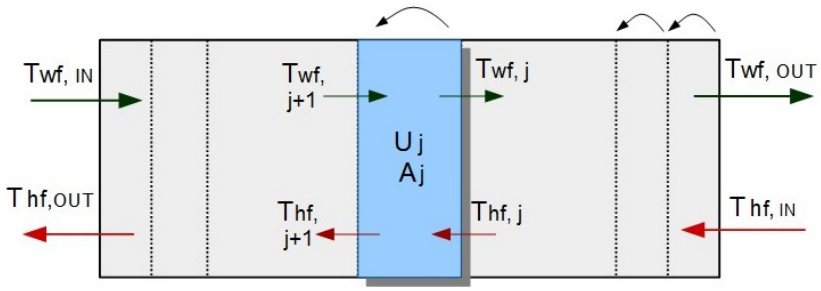


Figure 4.4: Sequential model of the heat exchanger. The generic element is highlighted.

For what concerns the mean temperature adopted to find $U_j$, we use again a guess value for $T_{wf,in}$ and $T_{hf,out}$ but now we suppose that the temperatures vary linearly inside the heat exchanger. This procedure leads to the definition of a mean temperature ($T_{m,j}$) for every element; the value of $T_{m,j}$ is then used in the evaluating of the physical properties during the $U$ calculation. The result of this strategy is a bigger accuracy in the calculation of the overall heat transfer coefficient.

The outputs of this model are the same of the first one. In fact, in the first section analysed (section 3 of the previous model) the evaporating temperature is given so the algorithm finds the number of elements needed to cool the vapour until saturated vapour ($n_3$); that is to say the area of zone 3. Moreover the corresponding temperature of the oil is evaluated ($T_{hf,3}$).
In the same way, can be calculated the temperature $T_{hf,2}$ and the heat transfer area of the second zone ($n_2$) ; that is because the latent heat of vaporization is known. Finally, the area of zone one is found as $n_1 = n - n_2 - n_3$. Using the heat transfer area and heat transfer coefficient, the temperatures $T_{hf,out}$ and $T_{wf,in}$ are evaluated.

The application of this method for the simulation of the heat exchanger produces a very stable behaviour and the convergence is almost always obtained. Moreover the precision of the results is quite good. For these reasons this we adopted this sequential method for the simulation of the two heat exchangers.

### 4.3.3 Model validation.

In this section we compare the results of the simulation to the experimental data. Using the data coming from the test rig, we prepared a set of input conditions to test the models. During this stage some small changes have

been made on the correlations coefficients, in order to obtain the best precision.
The performance of the model are evaluated considering the inlet temperature of the working fluid and the exchanged power. The indicators used are the percentage error and the temperature difference between the model and the real data.

### Evaporator

The evaporator inlet temperature obtained from the model is represented in Figure 4.5a. In this figure every point represents a different working point.
It can be observed that the agreement between the measurement and the prediction by the model is rather good. The error obtained for every point is represented in figure 4.5b, on the left-hand side. On the right-hand side the percentage error (PE) is illustrated.
The maximum deviation is 6.5° C, which corresponds to a percentage error around 2%; the mean absolute error (MAE) is 3.19° C corresponding to 1.25% of percentage error.

It can be interesting to evaluate the accuracy of the model even from the point of view of the thermal power exchanged. Figure 4.8 represents the power exchanged as a function of the mass flow rate of the working fluid. It can be noticed that the power exchanged is an increasing function of the mass flow rate. Moreover, two different levels of super-heating have been tested. For an higher value of super-heating the exchanged power is bigger, as expected. In fact, the pressure in the different points is quite similar and more heat is needed to heat the working fluid to an higher temperature.
Again, the agreement between experimental data and model is good. The maximum deviation is around 4.9% and the mean absolute error is 3.17%.

### Condenser

In the same way the condenser model have been validated over the experimental data. A set of working conditions have been use as input for the model and the obtain results have been compared with the measured temperatures and power.
The inputs parameters are: the mass flow of working fluid and cooling fluid, the organic compound outlet temperature and the cooling fluid inlet temperature. Again the pressure is assumed to be constant inside the eat exchanger.

The results obtained for the condenser inlet temperature are represented in figure 4.7a; Every point is a different working condition to validate the model. The agreement with the experimental data is quite good. The figure

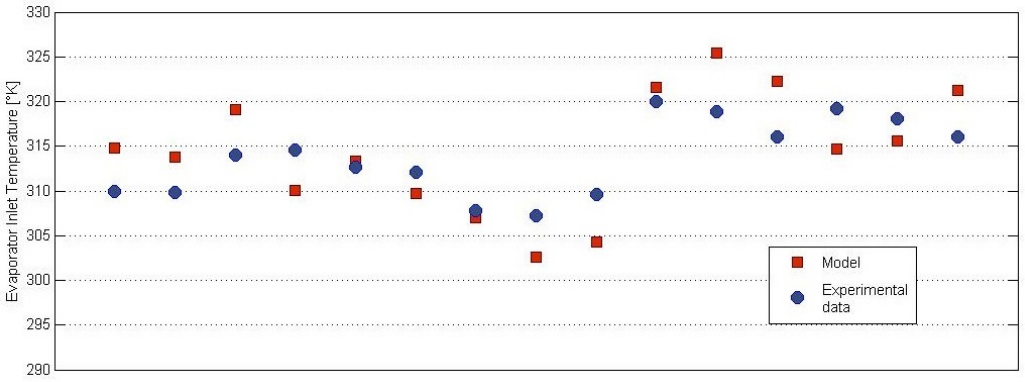


(a)

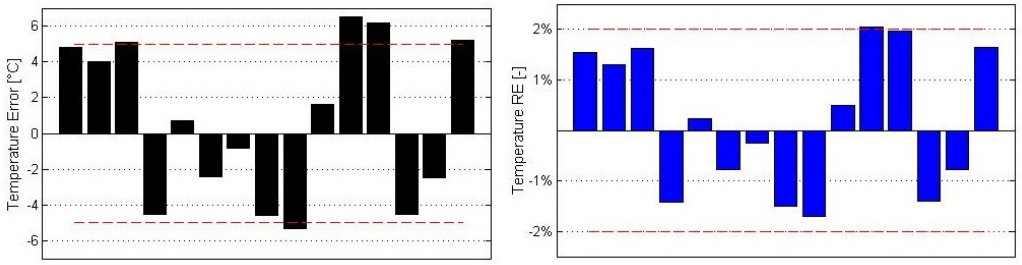


(b)

Figure 4.5: Evaporator inlet temperature: results from the model, experimental data and errors.

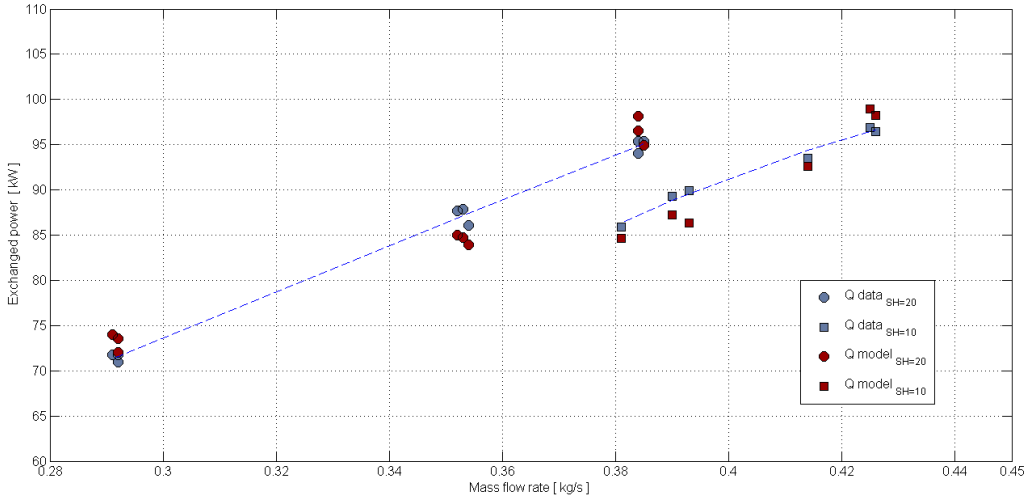


Figure 4.6: Thermal power exchanged in the evaporator as a function of mass flow rate and super-heating.

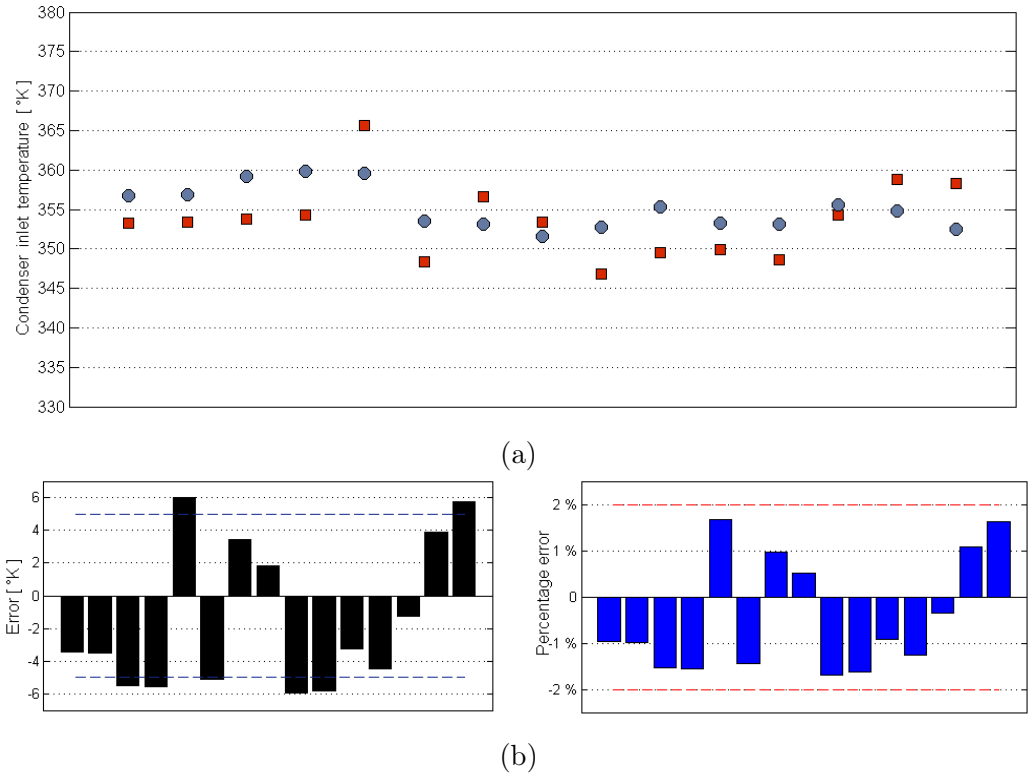


Figure 4.7: Condenser inlet temperature: results from the model, experimental data and errors.

below (Fig. 4.7b) represents the precision of the model, using the working fluid temperature as reference. In fact, the cooling fluid is subjected to a lower change in temperature so this error would be less meaningful.
The maximum temperature difference observed is around $6°C$, which corresponds to a percentage error smaller then 2%; the value of the mean absolute error is $4.13°C$ ( 1.2% in percentage).

The condenser have been evaluated even form point of view of the exchanged power. This parameter is shown in figure 4.8, as a function of the working fluid mass flow rate. The blue dots represent the experimental data while the red squares are the values coming from the model. As expected, the power is an increasing function of the mass flow rate; the value of the subcooling is almost always the same so just one branch appears. The maximum value of the percentage error is around 4% and its mean value is 2.3%.

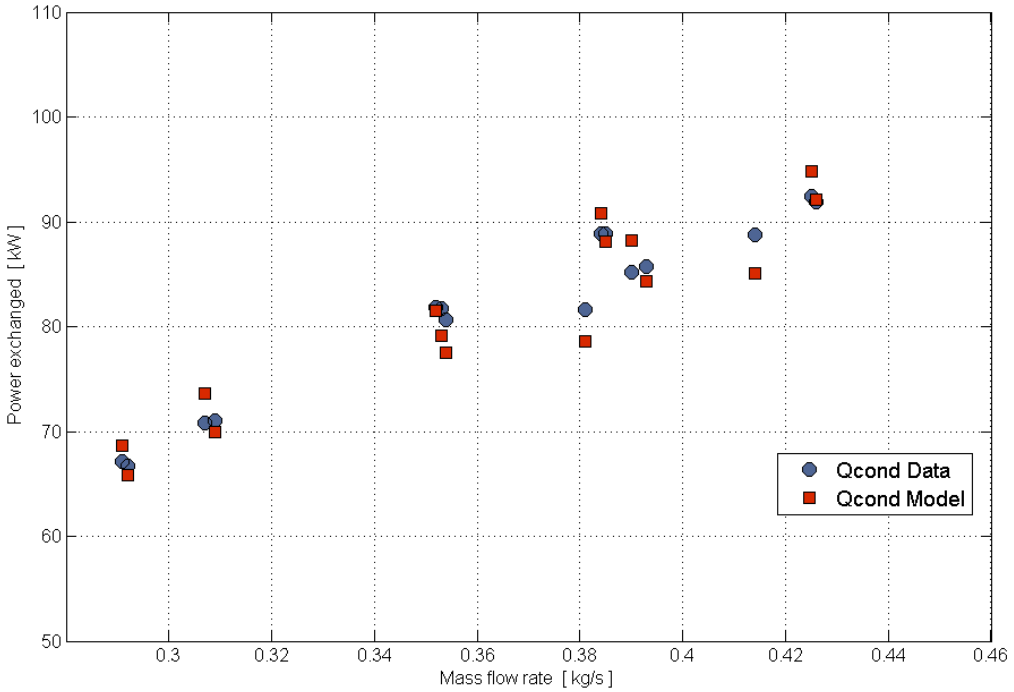


Figure 4.8: Thermal power exchanged in the condenser as a function of mass flow rate.

### 4.3.4 Conclusions.

In the end, a working heat exchanger model have been built and validated. The algorithm created proved to have the fundamental features of a good model: robustness and precision.
In fact the algorithm is capable of solving the temperature distribution for different input conditions and shows a stable behaviour over a reasonably wide range of guess values.

Moreover, the precision obtained can be judged satisfying, considering the simplifying hypothesis adopted. Since the main goal of a model like that is the evaluation of the steady state of the system, a percentage error minor then 5% can be considered acceptable. In fact, the global behaviour is well represented and the performance of the elements can be evaluated under different conditions.

A small remark can be made on the pressure. The accurate simulation of the pressure losses inside every element is not easy and rather time-consuming. For a steady state model an easier approach could be sufficient; for example, a fixed pressure loss can be supposed for every element. In particular, we tried to impose a constant pressure difference between the inlet and outlet of the heat exchanger and include it in the sequential model; this can be easily made assuming that the variation trough the elements is linear. However the results obtained are almost the same of the constant pressure model, so we decided not to change the model.

# Chapter 5

# System model and part-load analysis.

In this last chapter all the elements built and tested in the previous sections are assembled together in a complete model of the cycle. The main goal of this section is to validate a model of the whole ORC system and use it to draw a map for the part-load behaviour.

The first problem to face was the numerical formulation of the problem, in order to define the variables representing the cycle and obtaining a converging algorithm. Once this step was completed, the entire system model needs to be validated. This step is crucial to use this model as a tool for additional analyses.
Finally a part-load map is built, running the model over many different conditions; the results obtained are analysed and compared to the outcomes found in literature.

## 5.1 Construction of the system model.

We are now looking for a representation of the entire cycle. In order to do that it is necessary to define all the independent variables and reshape the models to combine one with the other.
First of all, we formulated a mathematical definition of the system, defining: the elements involved, the dependent variables and the independent variables.

The next step consisted in the numerical formulation of the problem. A first approach was completely "implicit"; in fact, all the variables and elements were coupled in a single system of equations. In a second step the algorithm used was "explicit", solving all the variables iteration by iteration.

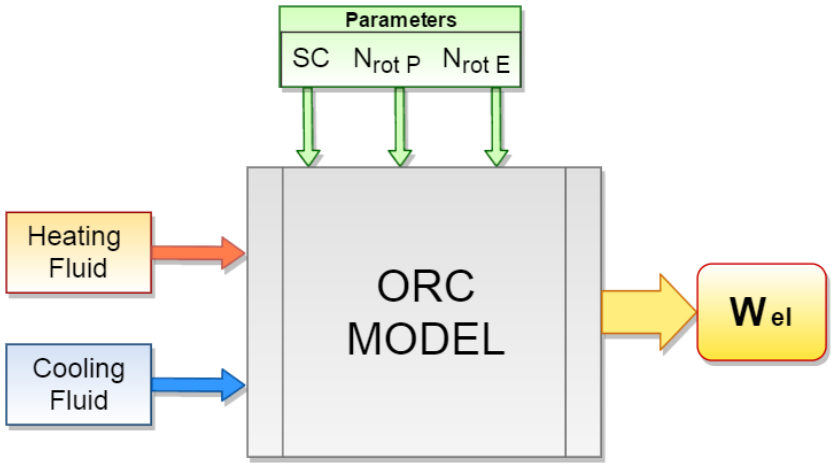


Figure 5.1: Schematic representation of the ORC model.

### 5.1.1 Mathematical definition of the problem.

As anticipated above, the goal of this study is to build a model able to calculate the power output for given external loops conditions and operating parameters. The external conditions of cooling and heating loops are represented using the mass flow rate and inlet temperature. The operating parameters used for the cycle are the pump rotational speed, the expander speed and the sub-cooling. A schematic idea of this model is represented in figure 5.1; this view underlines the model inputs and outputs.

In order to simplify the model, we decided to neglect the pressure losses, hence we consider only two pressures. In other words, we suppose that the pressure varies only inside pump and expander. All the elements from the pump outlet to the expander inlet are at the same pressure, called $P_1$; the other elements instead are at pressure $P_3$.
The independent variables that we have chosen are:

- the rotational speed of pump and expander
- the mass flow rate of the secondary fluids
- the inlet temperatures of the secondary fluids.

The dependent variables instead are:

- the evaporating and condensing pressure
- the mass flow rate of the working fluid

Table 5.1: Variables of the model.

| Independent variables | Dependent variables |
|---|---|
| $N_{rot,P}$ $N_{rot,E}$ | $P_1$ $P_3$ |
| SC | $\dot{m}$ |
| $T_{HF,in}$ $\dot{m}_{HF}$ | $h_1$ $h_3$ |
| $T_{CF,in}$ $\dot{m}_{CF}$ | |

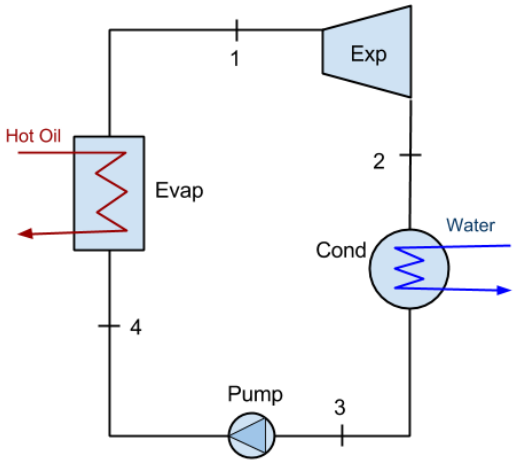


Figure 5.2: Schematic representation of the simple cycle.

- the enthalpies of the working fluid after the condenser and after the evaporator.

Referring to the numbers in figure 5.2, the dependent and independent variables are resumed in table 5.1.

The other two values of enthalpy (before the pump and before the expander) can be easily computed when the system of equation is solved. They are implicit in the system because the enthalpies in points 2 and 4 are required to have the same value. In other words, the value of enthalpy leaving the pump should be the same of the one entering in the evaporator. In the same way, the enthalpy coming out of the expander should equal the enthalpy entering the condenser.

The models built in the previous sections have been rearranged in specific functions, in order to be coupled. For every function the independent variables and output variable are listed in table 5.2.

Table 5.2: List of the elements used in the system.

| Function | Independent variables | Result |
|---|---|---|
| Evaporator | $P_1$, $h_1$, $\dot{m}$, $\dot{m}_{HF}$, $T_{in,HF}$ | $h_4$ |
| Condenser | $P_3$, $h_3$, $\dot{m}$, $\dot{m}_{CF}$, $T_{in,CF}$ | $h_2$ |
| Expander Mass | $P_1$, $P_3$, $h_1$, $N_{rot,E}$ | $\dot{m}$ |
| Expander Enthalpy | $P_1$, $P_3$,$h_1$,$\dot{m}$, $N_{rot,E}$ | $h_2$ |
| Pump Head | $P_3$, $h_3$, $\dot{m}$, $N_{rot,P}$ | $P_1$ |
| Pump Enthalpy | $P_1$, $P_3$, $h_3$, $N_{rot,P}$ | $h_4$ |

Now the system of equations can be finally set up.

$$\begin{cases} Evaporator(P_1, h_1, \dot{m}, \dot{m}_{HF}, T_{in,HF}) = PumpEnthalpy(P_1, P_3, h_3, N_{rot,P}); \\ Condenser(P_3, h_3, \dot{m}, \dot{m}_{CF}, T_{in,CF}) = ExpanderEnthalpy(P_1, P_3, h_1, \dot{m}, N_{rot,E}); \\ \dot{m} = ExpanderMass(P_1, P_3, h_1, N_{rot,E}); \\ SC = T_{evap}(P_1) - T_3(h_3, P_3) \\ P_1 = P_3 + PumpHead(P_3, h_3, \dot{m}, N_{rot,P}). \end{cases}$$

This system is solved using the solver *fsolve* in Matlab, used for systems of non-linear equations. The algorithm used is the trust-region algorithm. Our code receives as inputs the data of external loops and rotational speed from the experiments and use some guess values to initialize the solution.

Even if the problem appear to be complete, the computational solution hardly ever converges. In fact, during the validation process, a very good guess was needed to obtain convergence of the solution. If the initial value provided is not good enough the solution process rapidly diverges.
However, it is not easy to understand the influence of the various variables involved and it could be hard to provide a good guess value. This problem is critical because it doesn't allow for extrapolation beyond these working conditions.

Some changes have been made on the solver options to deal with this problem. First of all, two other algorithms have been tested (the trust-region reflective algorithm and Levenberg-Marquardt algorithm). However the solution obtained presents the same problem of instability. Even relaxing the tolerances used by the solver the result doesn't change.

### 5.1.2 Solution method.

Since the implicit mathematical formulation of the problem showed so many problems of convergence, we decided to develop an explicit approach. In

fact, in using the system of equation all the variables are implicit and it is not possible to control the solution process. In the second approach instead, an iterative solution process have been implemented. Even if the variables and function used are the same of the first solution method, now the variables along the cycle are solved sequentially.

Three iteration cycles have been built: one cycle to find the value of evaporating pressure, one for the condensing pressure and the last for the super-heating value. The flow chart of this solution process is represented in figure 5.3.
Fist of all, three guess values are provided for the pressures and super-heating (starred in the figure). The most internal loop is represented in figure 5.4a; this iteration cycle is used to find the value of $P_1$, for a given condensation pressure and super-heating. The filling factor model of the expander also provides the mass flow rate of the working fluid, for a given rotational speed ($N_{rot,E}$). The values of $h_1$ and $h_3$ directly follow from the guess values of pressures, super-heating and sub-cooling.

In the second cycle the super-heating is calculated (see figure 5.4b). The values of $P_1$, $P_3$ and $h_3$ are used inside the pump efficiency model to find the enthalpy at the evaporator inlet ($h_4$). Now an iteration process is used to adjust the value of super-heating until the value of $h_4$ calculated by the evaporator doesn't match the one obtained by the pump. In this way the influence of the heating conditions are included in the model. The results of this section are the super-heating value and evaporator inlet enthalpy value. The process is far more stable then the direct solution of the equation system. In fact, the input for the evaporator model is sequentially changed, through small steps. In the implicit process instead, a large variation could occur, ending up in an unstable point. That is because the models are very "sensible" and even a small change in the input data creates a big variation in the output.

Finally the external cycle calculates the condensing pressure and is represented in figure 5.4c. The process used here is very similar to the previous cycle. In fact, the variables already calculated ($P_1$,$P_3$,$h_1$,$\dot{m}$) are used in the expander efficiency model to find the value of the expander exhaust enthalpy ($h_2$). Now this value is set as a target in the condenser model. Since the value of sub-cooling is given, choosing a value of evaporating pressure correspond to set the enthalpy $h_3$. Therefore, $P_3$ is modified step by step until the correct inlet enthalpy is achieved. This last step takes into account the influence of the cooling conditions.
The same considerations made on the stability of the evaporator can be repeated here.

In the end, the result obtained is a stable and quite easy model, able to converge even if the initial guess values are not so precise. Even the computational time is shorter. The goodness of the results obtained is evaluated in the next section.

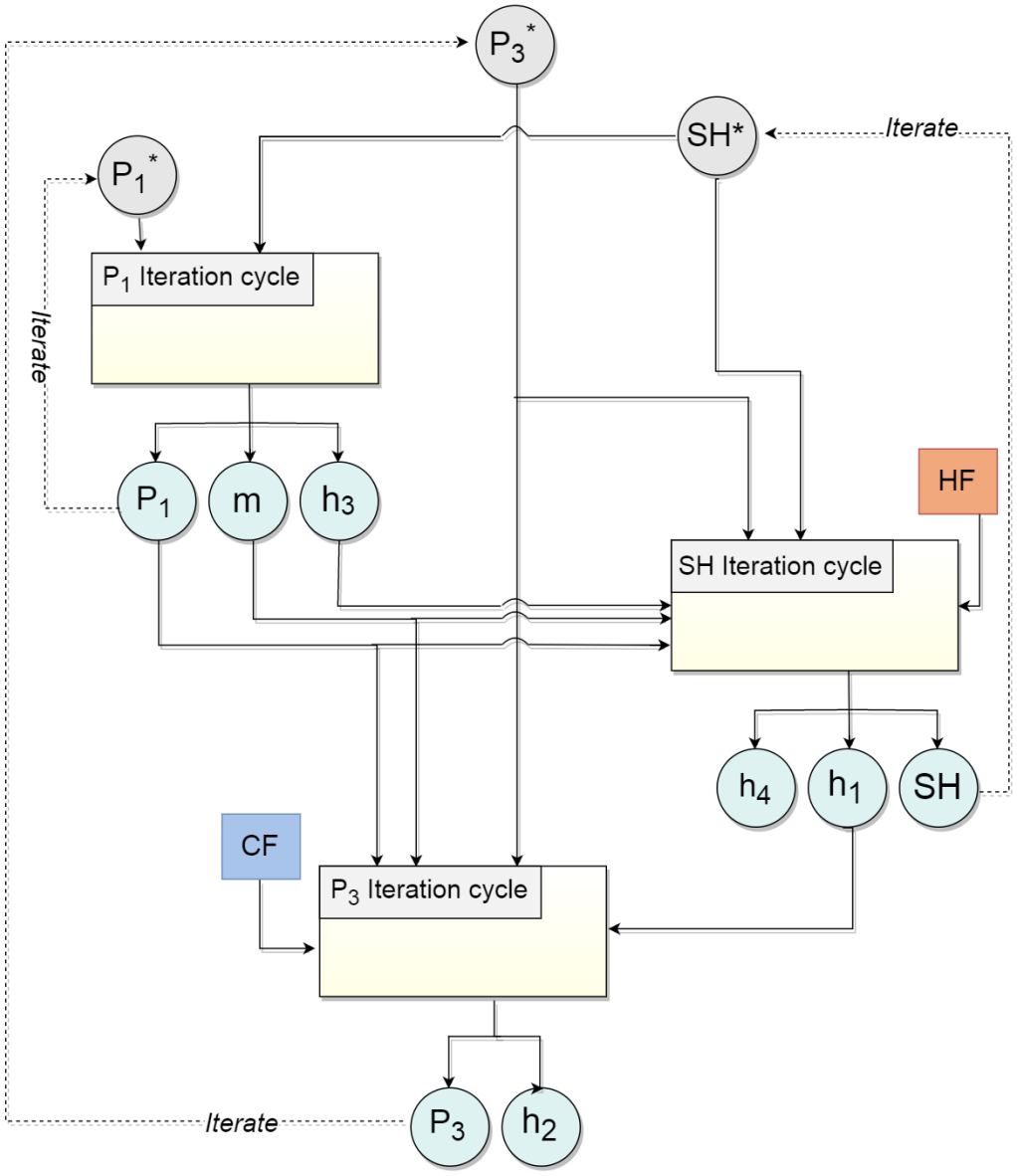


Figure 5.3: Flow chart representing the iterative solution process.

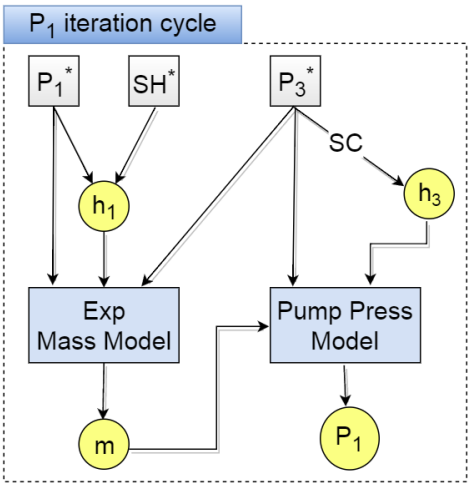


(a) Iteration cycle to find $P_1$

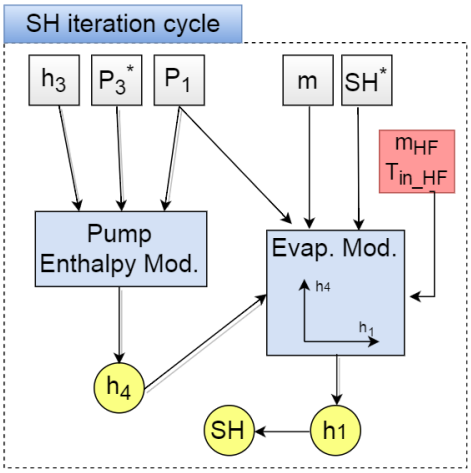


(b) Iteration cycle to find $SH$

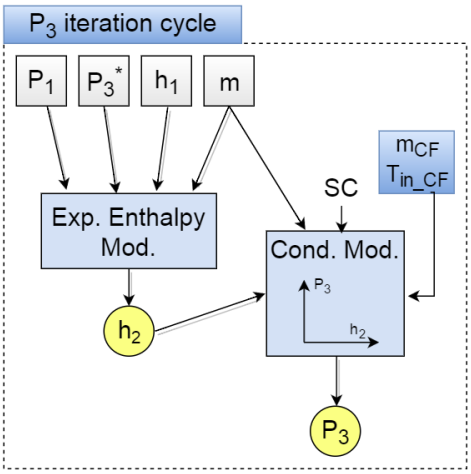


(c) Iteration cycle to find $P_3$

Figure 5.4

## 5.2 Validation of the model.

Once the system model is complete, the results obtained are compared to the experimental data. In fact, it is crucial to prove the reliability of the model before any other analysis.
The test conditions are the same described in chapter 2. In particular, the external loops conditions are resumed in table 5.3 and 5.4. Unfortunately, the number of different conditions analysed is quite small and it doesn't allows to cover a very wide range of possibilities. However, these points appear to be sufficient to test the goodness of the model in different part-

| Heating loop | |
|---|---|
| $m_{hf}$ $kg/s$ | $T_{hf,IN}$ $^{\circ}C$ |
| 1.5 | 110 |
| | 120 |
| 2.1 | 120 |
| 3 | 110 |
| | 120 |

Table 5.3

| Cooling loop | |
|---|---|
| $V_{cf}$ $m^3/h$ | $T_{cf,IN}$ $^{\circ}C$ |
| 7 | from 27.8 to 35.1 |
| 13.5 | from 28.2 to 38.2 |
| 19.5 | from 29.5 to 38.0 |

Table 5.4

load conditions. The results are analysed using the parity plot representation and the percentage relative error.

The code created in *Matlab* receives as input the external loops conditions and the parameters values and returns the values of enthalpy, temperature and pressure in all the four points of the cycle. Moreover, the model can draw:

- the $T-s$ diagram of the cycle, including the water and oil temperatures;
- the heat transfer process of evaporator and condenser. They are represented in a power-temperature diagram $Q-T$;
- the entropy-temperature $T-s$ diagram of the expansion process.

The last two elements are represented in figure 5.5 for an example working point and represent a quick tool of comparison. In each one of these plots the predicted value obtained from the model have been compared to the experimental data. The predicted value is represented by the solid lines while the experimental data by the dashed ones. It is immediately clear that the accuracy of the results is very good, and the solid lines adequately follow the dashed ones.

An additional comparison have been proposed using the parity plot and the absolute relative error. The parity plot for expander power and cycle efficiency are represented in figure 5.6a and 5.6b.

The precision of the absolute relative error have been evaluated on the results obtained for pressure, mass flow rate, temperature and electrical power output. The maximum and mean value of the absolute relative error are represented in table 5.5.
All the values are very good and denote a satisfying agreement in all the

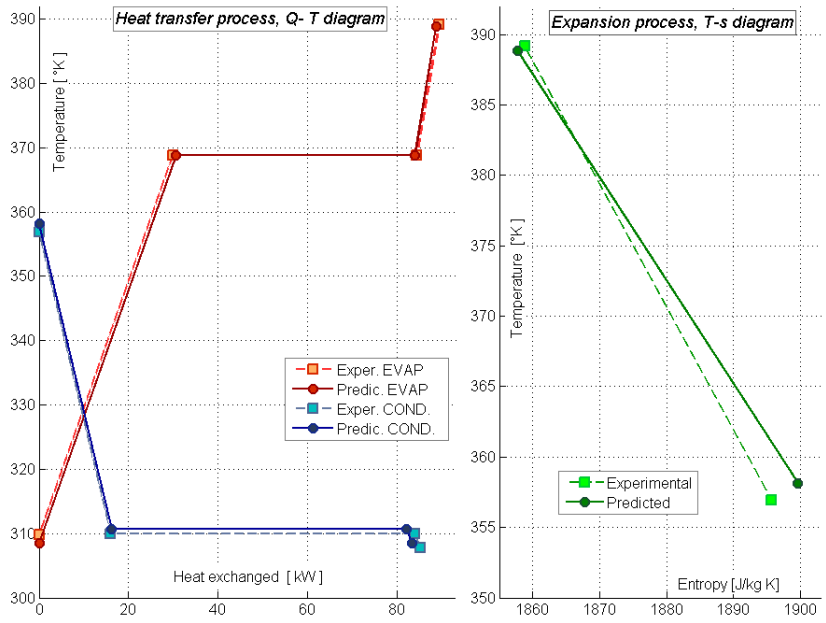


Figure 5.5: Example of QT diagram of the heat exchangers(left), and Ts diagram of the expansion process (right).

points evaluated. The only significant variation can be identified at lower super-heating values. In fact, two different levels of super-heating have been tested: 10 and 20°$C$. When the super-heating is lower the relative error is bigger. In particular, shifting from 20 to 10 degrees of super-heating, the mass flow rate increases as expected, but its value is still smaller then the experimental value. The evaporating pressure also shows a more considerable error in this condition; obviously these errors affect also the precision of the expander power, which appears bigger then the actual value. The maximum values of relative error are all located in this part of the data set.

However, it was not possible to find any particular explanation to this phenomenon. In fact, the behaviour of the entire cycle is quite complicated to understand and the test conditions were always variable; the water inlet temperature for example was influenced by the external ambient temperature and it wasn't possible to set a precise value. A wider and more complete experimental campaign would be necessary to understand the reason of this behaviour and to investigate the precision on the model for other values of super-heating. Looking at the table of relative error the maximum value is connected to the expander power; this could be due to the error propagation, involving the mass flow rate value and the pressure value.

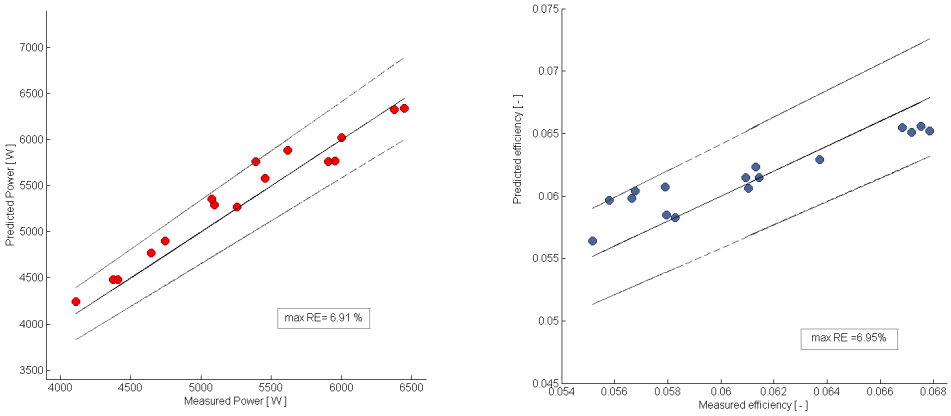


(a) Expander power: parity plot. (b) Cycle efficiency: parity plot.

Figure 5.6

Table 5.5: Validation of the model: maximum and mean value of the absolute relative error.

| Variable | Absolute relative error | |
|---|---|---|
| | mean | max |
| Evap. Pressure | 0.73% | 2.67% |
| Cond. Pressure | 0.75% | 1.78% |
| $T_1$ | 1.06% | 1.44% |
| $T_2$ | 1.35% | 2.12% |
| $T_3$ | 1.96% | 3.42% |
| $T_4$ | 3.57% | 5.28% |
| Mass flow rate | 0.96% | 3.58% |
| Electric power | 2.81% | 6.91% |

An additional representation of the power is proposed in figure 5.7. This 3D surface represents the value of the expander power predicted by the model in the different conditions tested. The heating loop conditions are represented by the power $Q_{EVAP}$ while the cooling loop conditions are represented by $T_{CF,IN}$.
The blue points in the figure represent the experimental data for $W_{exp}$ and appear to be very close to the predicted surface.

In conclusion, we obtained very good results from the validation of the cycle model on the available points; the values of relative error remained always quite small and the agreement to the experimental data was good

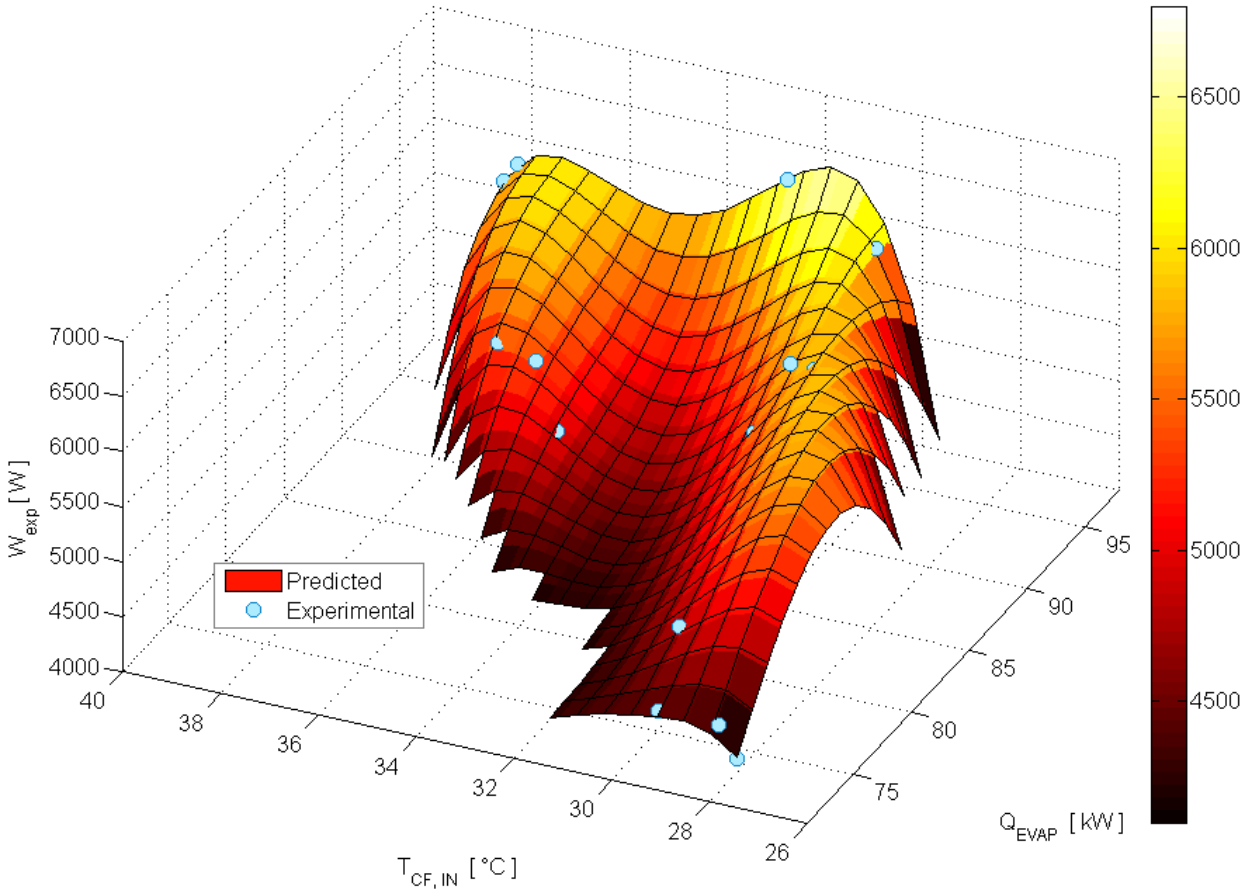


Figure 5.7: Expander power validation: 3D surface.

in all the test conditions. However, a criticism can be made on the number of points used to validate the model. A more accurate work can be done testing the model on a wider range of conditions. From the other hand, it was not easy to set up a good experimental campaign and understand the more significant conditions to test in the short period available. A more accurate research activity would have probably required more time.

## 5.3 Part-load regime.

Now that the model is finally complete and validated, it could be used as a valid tool to investigate the performance of the cycle in part-load conditions. Investigating this behaviour is very important from many points of view and many studies have been proposed on this matter.

In order to design a cost-effective cycle is essential to set an optimization method. Many different criteria can be found in literature. For example, Hettiarachchi et al. [30] presented a design strategy for a binary Organic Rankine power cycle using low-temperature geothermal resources. The evaporation and condensation temperatures and the geothermal and cooling water mass flow rates were varied in order to find the optimal cycle sizing. The article of Macián et al. [43] describes a methodology for the optimization of a bottoming cycle as a waste heat recovering system in vehicles. The working fluid and the heat exchanger area are found as a function of the heat source conditions.

In the above papers the simulations were performed in a nominal working point. However, it is important to take part load regime into account as operating conditions can vary strongly over a year.
An important step in this direction was proposed by Lecompte et al. [37]. A methodology is proposed to select a thermo-economic optimal design for an ORC under changing operating conditions. Following the same approach we have tried to obtain a part-load map for the analysed cycle, representing the electrical power output under different external conditions.

Simulating the part-load behaviour is understanding the connection between the external conditions of cooling and heating loops and electrical power produced by the cycle, outside the nominal condition.
This approach is very important to obtain the best thermo-economic design, considering the real working parameters. Moreover, it can be possible to implement a better control strategy following this approach.

Table 5.6: First set of operating points.

| $m_{HF}$ $kg/s$ | $T_{HF,IN}$ $°C$ | $V_{CF}$ $m^3/h$ | $T_{CF,IN}$ $°C$ |
|---|---|---|---|
| $1.7-3.4$ | 110 | | |
| $1.3-3.5$ | 120 | 35 | 13 |
| $1.3-2.2$ | 130 | | |
| 2 | 110 | $6-20$ | 25 |
| | | $7-21$ | 30 |
| | | $5.5-21$ | 35 |
| | | $7-23$ | 40 |

### 5.3.1 Testing the model under part-load conditions.

The performance of the cycle was evaluated under different operating conditions, changing the mass flow rate and inlet temperature for heating and cooling fluid. In this first section, the more representative parameters of the cycle have been evaluated in different points.

In this process the values of super-heating and sub-cooling have been set to 10 and $2°C$ respectively. The expander rotational speed is set to $5000rpm$ while the value of the rotational speed of the pump needs to be found.
Every point has a different external loops condition. Three different temperature have been tested for the heating fluid inlet; for each temperature, the mass flow rate of the oil has been changed gradually. The cooling fluid conditions are fixed. The same process has been repeated for the cooling loop: for a fixed heating fluid condition, four water inlet temperatures have been tested, adjusting the volumetric flow. The operating points tested are resumed in table 5.6.

#### Pressure.

Let us consider the pressure obtained from the cycle in the different points. The figure 5.8 represents the evaporating and condensing pressure of the working fluid. The evaporating pressure is plotted as a function of $\dot{m}_{HF}$, for three values of inlet temperature $T_{HF,IN}$ (see 5.8a).
The value of pressure strongly increase when the inlet temperature rises. For example, setting the heating fluid mass flow rate to $2kg/s$ and increasing the temperature from $110°C$ to $130°C$, the pressure varies from 10 to 14.2 bar. This is obviously what we expected because, fixing the super-heating, the evaporating temperature should follow the inlet temperature and so does the pressure. Anyhow, it could be interesting to notice the influence of the

heating fluid mass flow rate. In fact, when $T_{HF,IN}$ is low the pressure remains almost constant, when $T_{HF,IN}$ is higher instead, the evaporating pressure is an increasing function of the $\dot{m}_{HF}$.

This phenomenon could be explained as follows: when the inlet temperature value is equal to $110°C$ we are close to design conditions and the temperature difference in the exiting section is low; when $T_{HF,IN}$ is higher instead, this difference is bigger. Now rising the mass flow rate of the heating fluid the heat exchanger performance improves, reducing the pinch-point value. A bigger value of $T_{HF,IN}$ allows a larger improvement in the pinch point and thus a larger increase in evaporating temperature and pressure.

The condensing pressure is plotted in figure 5.8b. Here both inlet temperature ($T_{CF,IN}$) and volumetric flow of the cooling fluid ($V_{CF}$) significantly influence the pressure. In fact, for a given volumetric flow, a $15°C$ drop in the inlet temperature cause the evaporating pressure to decrease around 1.2 bar; the influence of $V_{CF}$ on this drop is very small.
The curve trend of $P_3$ as a function of $V_{CF}$ for a given inlet temperature is more or less quadratic; for low values of volumetric flow the rate of change is bigger and decreases at higher values.

Obviously, reducing, the water inlet temperature it is possible to obtain a lower condensing temperature and pressure. The same effect can be achieved with a larger mass flow rate. However, the influence of this parameter is not simply linear because a bigger mass flow rate, from one hand, increases the heat exchange coefficient but from the other, it also increases also the heat capacity of the cooling flow, reducing the temperature different in each section. These two opposing effects result in a non-linear influence on $T_{cond}$ (and thus on $P_3$).

**Mass flow rate.**

Also the mass flow rate of the working fluid is analysed for the different operating conditions. The parameters used to plot the mass flow rate is the power supplied and removed in the evaporator and condenser respectively. These are considered representative of the external loops condition.

The value of the mass flow rate as a function of the evaporating power is represented on the left-hand side of figure 5.9. As expected, the value of $\dot{m}_{WF}$, strongly depends on the heating loop conditions. Moving from the minimum value of $Q_{EVAP}$ (corresponding to $\dot{m}_{HF} = 1.7$ and $T_{HF,IN} = 110°C$) to the maximum ($\dot{m}_{HF} = 2.2$ and $T_{HF,IN} = 130°C$), the mass flow rate strongly

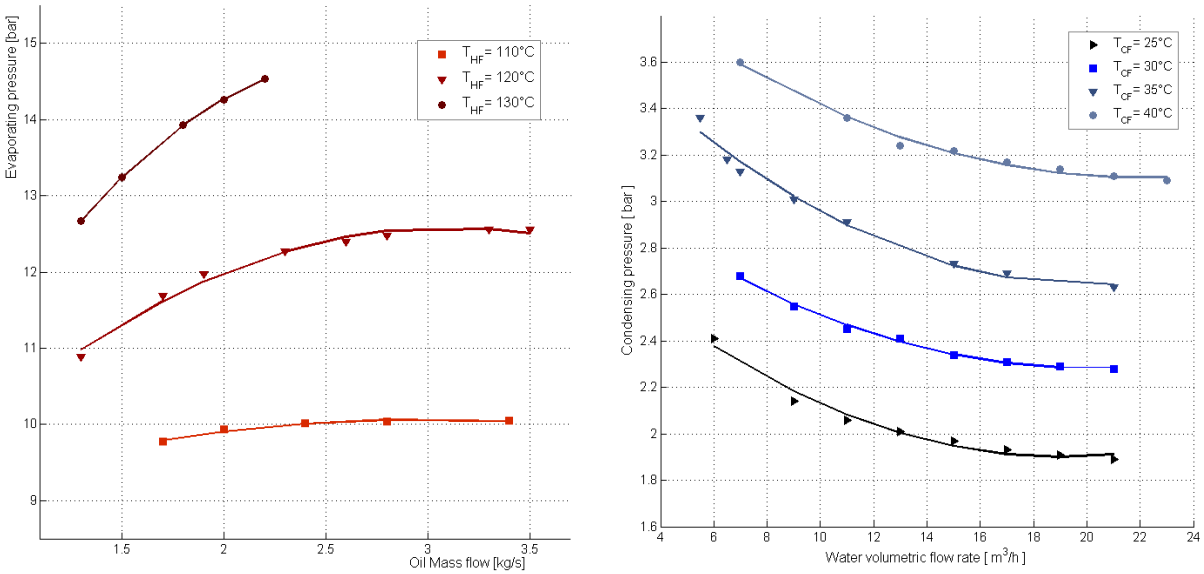


(a) Evaporating pressure.

(b) Condensing pressure.

Figure 5.8

increases: from 0.3 to 0.45 $kg/s$.
This behaviour is due to the fixed cooling conditions. In fact, fixing the value of sub-cooling, the cooling fluid volumetric flow and temperature causes the evaporator inlet temperature to be almost constant. From the other hand, the evaporator outlet temperature is limited by the oil inlet temperature. Therefore, the only way to absorb a bigger power is increasing the mass flow rate of the working fluid.

On the right-hand side of figure 5.9 the variation of mass flow rate is represented as a function of the condensing power $Q_{COND}$. Here the influence of the external conditions is very low and the mass flow rate change is less then 0.02 $kg/s$. When the volumetric flow rate of the cooling flow rises or the inlet temperature decreases, the value of $Q_{COND}$ grows and $\dot{m}_{WF}$ slightly diminishes.

**Power.**

Finally the cycle power is analysed. This is considered to be the most important parameter to evaluate the performance of this kind of systems. In fact, in heat-recovery applications the output power is generally more important then the efficiency.
This analysis follows a generic approach and it is focused on the cycle only;

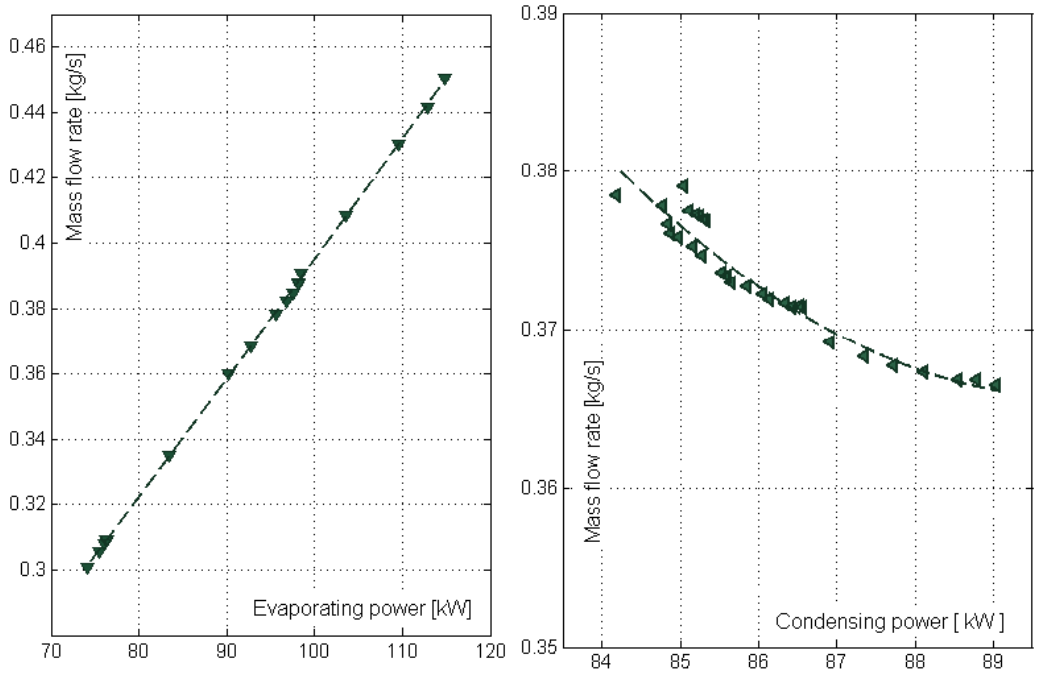


Figure 5.9: Mass flow rate as a function of evaporating power (on the right-hand side) and condensing power (on the left-hand side).

the power consumption of the secondary loops is not considered. Therefore, the values of power that we refer to are the expander power and pump power.

The trend of expander power and net power (expander - pump) are shown in figure5.10 in order to understand the influence of the part-load conditions on the power output.
The plot 5.10a considers the influence of the heating fluid condition in terms of $\dot{m}_{HF}$ and $T_{HF,IN}$. The figure 5.10b instead represents the expander and net power as a function of $Q_{COND}$. The net power $W_{net}$ is strongly influenced by the heating fluid inlet temperature, while the influence of mass flow rate is relevant only for higher temperatures. That is because the expander inlet pressure and mass flow rate follow this behaviour, as shown in the previous paragraphs.

The electrical power shows a linear dependence on the thermal power supplied (see fig. 5.10b). Changing the heating loop conditions the electrical power growth is remarkable.
In particular, it is interesting to distinguish between the expander and net power. The increase of electrical power produced by the expander is due to a bigger mass flow rate of the working fluid and to a larger value of the inlet

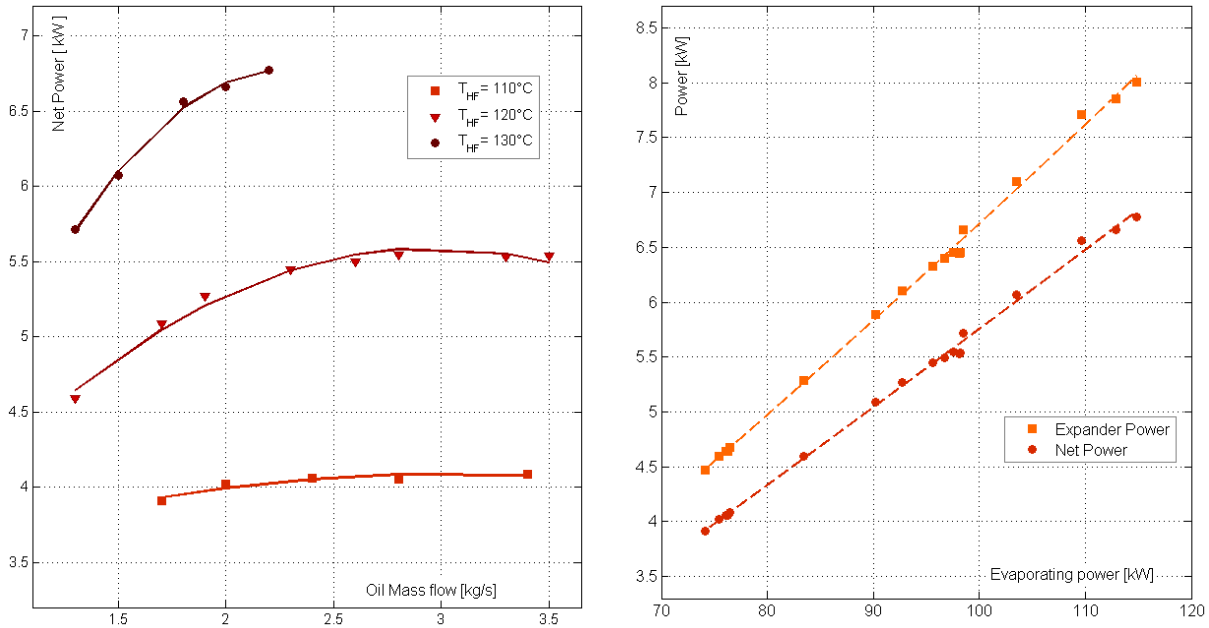


(a) Net power output for different $\dot{m}_{HF}$ and $T_{HF,IN}$.

(b) Expander and net electrical power as a function of $Q_{EVAP}$.

Figure 5.10

enthalpy (because both temperature and pressure are larger). Anyhow, when the mass flow rate increases also the power absorbed by the pump increases, lessening the net power growth.

The influence of the cooling conditions are represented in figure 5.11. The figure 5.11a in particular shows the influence of $\dot{V}_{CF}$ and $T_{CF,IN}$ on the net power output. The trend is complementary to the evaporating pressure behaviour: the lower is the inlet temperature and the higher is the power output. The influence of volumetric flow exhibits a quadratic trend, similar for every temperature.
The behaviour of the condensing pressure together with the almost constant value of the mass flow rate, results in the trend shown in figure 5.11b. In fact, the expander and net power are not linearly dependent on the power exchanged in the condenser $Q_{COND}$. For low values of $Q_{COND}$ the electrical power exhibits a strong growth, for higher values instead the electric power lessens its improving.
The influence on the pump power is more complex to distinguish in this case. In fact, the mass flow rate diminishes but really just a few. The value of the pressure difference instead arises considerably. The heating conditions, in

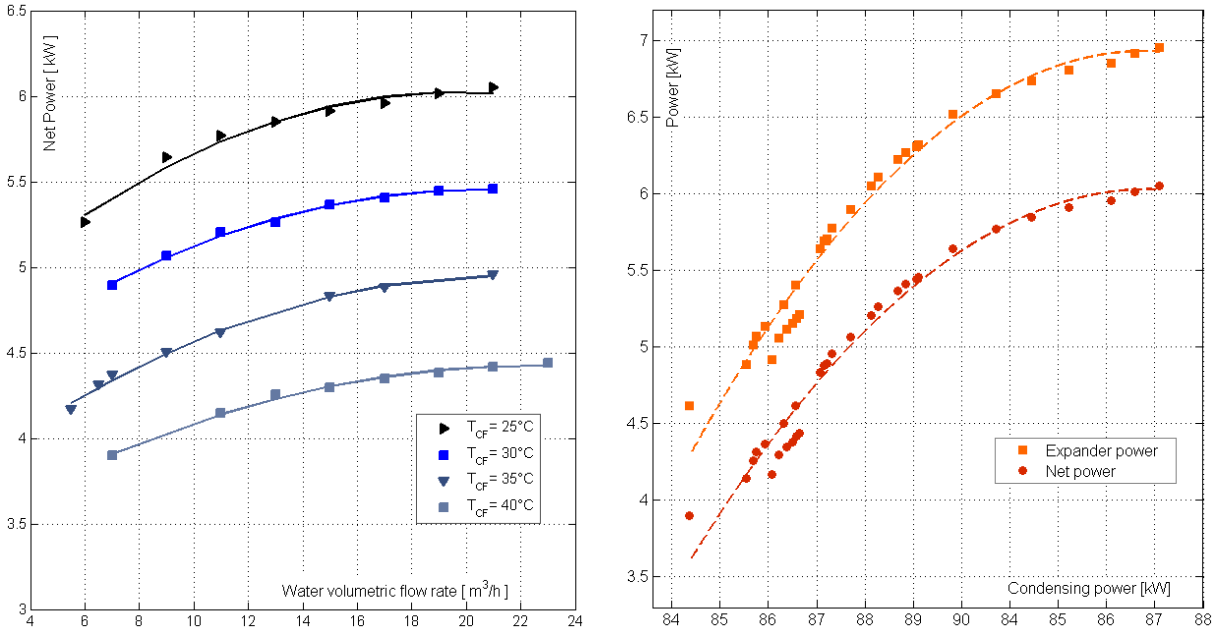


(a) Net power output for different $\dot{V}_{CF}$ and $T_{CF,IN}$.

(b) Expander and net electrical power as a function of $Q_{COND}$.

Figure 5.11

fact, are maintained fixed in this test and so is the pressure $P_1$; the value of $P_3$ instead drops when $Q_{COND}$ arises. The result is a larger power absorbed by the pump, even if its value diminishes in percentage of the expander power.

### 5.3.2 Part-load maps.

As suggested in the article of Lecompte et al. [37], it could be use useful to represent the part-load behaviour of the cycle using a map. This is an easy tool to quickly visualise the performance of the cycle when the external loops conditions change. Moreover, comparing our maps with the maps in the article could be an additional demonstration of the physical coherence of our results.

The maps that we present are based on additional test conditions, in order to cover a complete range of test conditions. The variables used to draw the maps are the thermal power exchanged in the evaporator $Q_{EVAP}$ and the cooling fluid inlet temperature, $T_{CF,IN}$.
The figures 5.12 and 5.13 show the variation of the expander power and cycle net power respectively. The colour of the maps are proportional to the

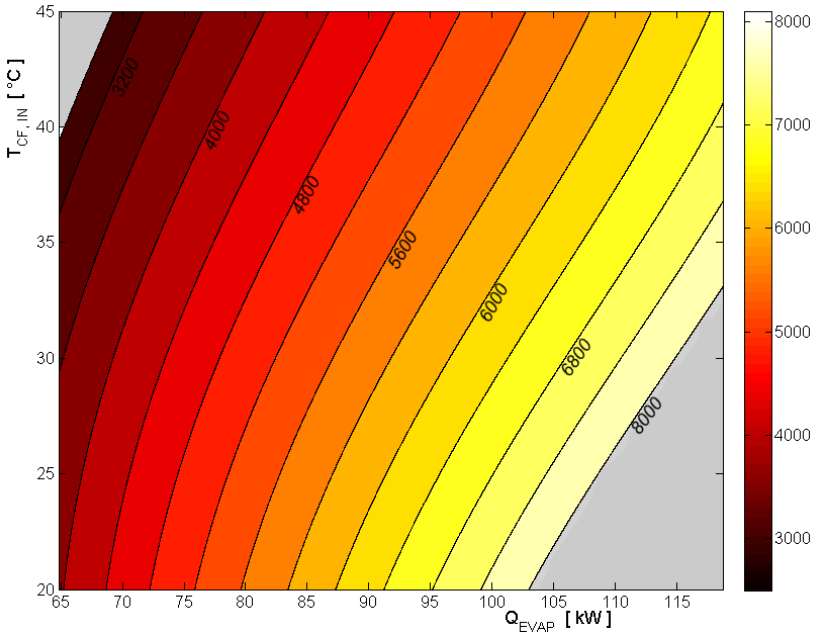


Figure 5.12: Expander power map as a function of $T_{CF,IN}$ and $Q_{EVAP}$.

value of power expressed in $W$. The maximum value of expander power is equal to 8020 $W$ and it is obtained for the minimum value of water inlet temperature ($20°C$) and maximum value of $Q_{EVAP}$ ($\dot{m}_{HF} = 1.3kg/s$ and $T_{HF,IN} = 130°C$). It was not possible to obtain a satisfying convergence for a mass flow rate larger then 2.2 $kg/s$.
The minimum power that can be achieved is 2990 $W$ and correspond to the opposite external loops conditions: $T_{CF,IN} = 45 \circ C$, $\dot{m}_{HF} = 1.2kg/s$ and $T_{HF,IN} = 110°C$.

The map of the ORC net power is represented in figure 5.13. The shape of this function is very similar to the expander power. The minimum and maximum values of the net power generated by the ORC obviously occur in the same conditions of the minimum and maximum expander power. The maximum value is 6936 W and the minimum value is 2599 W.
As we discussed above, the pump power is mostly influenced by the thermal power exchanged in the evaporator while the influence of $T_{CF,IN}$ is very low. For this reason the net power curve presents the same shape of the expander power curve, it is just shifted. The 3D representation of these surfaces are shown in figure 5.14. The expander power is marked with solid lines, the net power using dashed lines.

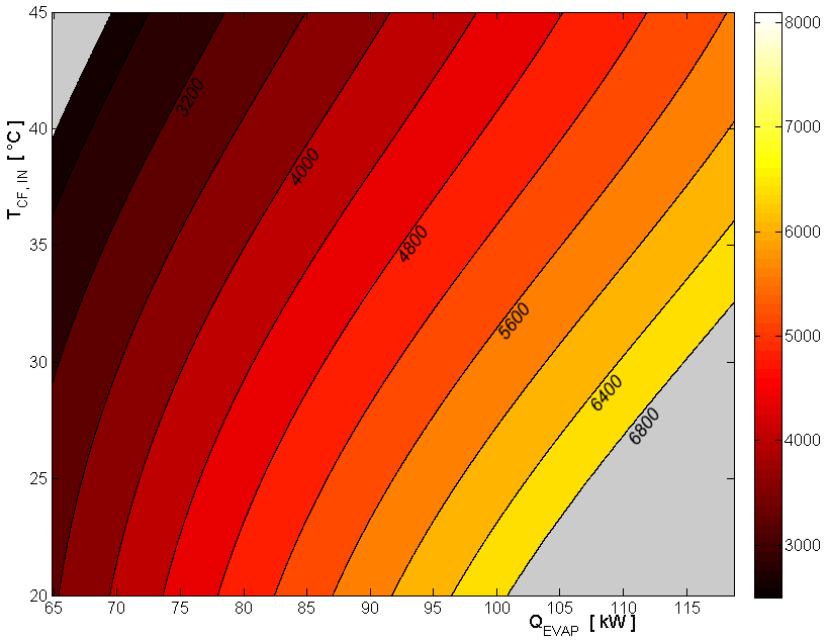


Figure 5.13: ORC net power map as a function of $T_{CF,IN}$ and $Q_{EVAP}$.

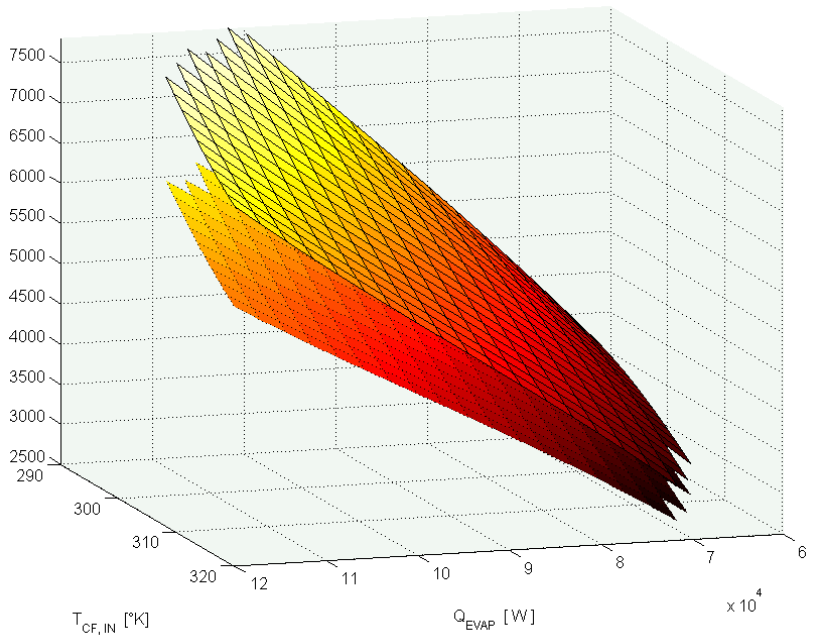


Figure 5.14: 3D surface of $W_{exp}$ and $W_{net}$ as a function of $T_{CF,IN}$ and $Q_{EVAP}$.

**Efficiency.**

As we have already explained, the performance of the cycle was analysed only from the point of view of the power output. First of all, this is considered to be the most important parameter to optimize in a heat recovery power plant. Moreover in the analysis that we perform it was not possible to evaluate the power absorbed by the auxiliaries in the external loops. For all these reasons the evaluation of the cycle efficiency is not as complete as it should be and it is just an indication of the relation between the power generated by the expander and the power absorbed by the pump.
The map of the efficiency is represented in figure 5.15. The maximum and minimum values of efficiency are situated in the same maximum and minimum points cited above; their values are respectively 8.8% and 5.6%.

As it is shown in the figure, the influence of external conditions on the efficiency is quite different from what we have seen on the power output. In fact, comparing the isolines of efficiency and power it can be noticed that the slope of the lines in the power map is steep and quite constant. That indicates that the influence of $Q_{EVAP}$ is larger than the influence of $T_{CF,IN}$. In the efficiency map instead, the slope of the isolines is quite steep when the value of $Q_{EVAP}$ is lower and tend to decrease for higher values of evaporator power. This behaviour can be explained as follows: when $Q_{EVAP}$ grows the mass flow rate of the working fluid increases as well; this causes an increment in the power produced by the expander but also in the power absorbed by the pump too; the increase of efficiency is thus reduced.
This tendency would probably be enhanced if we considered the auxiliaries power. In fact, when the oil mass flow rate rises also the power absorbed by the heating loop pump increases. Therefore, for higher values of $Q_{EVAP}$ the slope of the isolines would show a further drop.
The behaviour that we have just supposed it is the same that can be found in the work of Lecompte et al. [37].

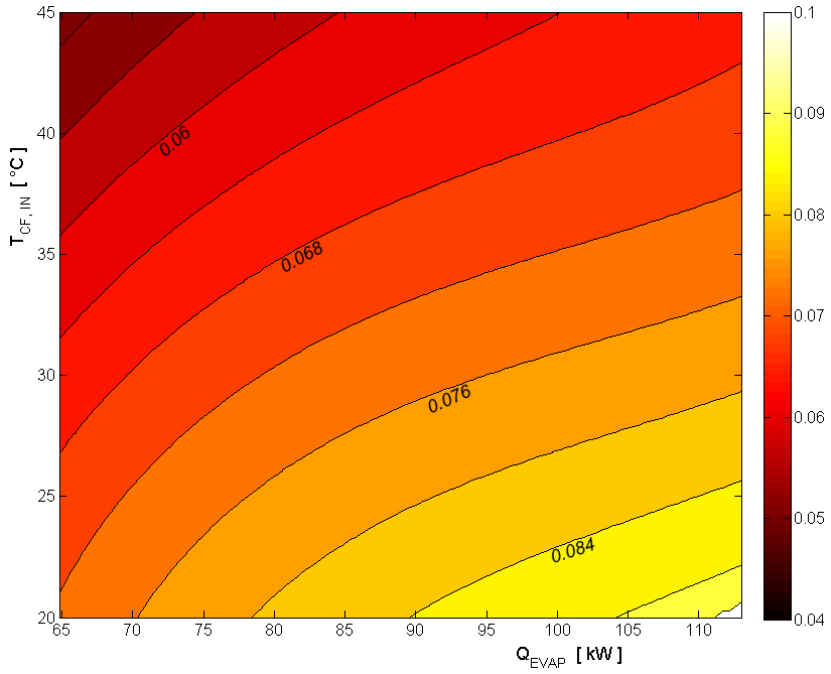


Figure 5.15: Efficiency map as a function of $T_{CF,IN}$ and $Q_{EVAP}$.

# Chapter 6

# Conclusions.

The main achievement of this thesis is the development of a generic model for the part-load behaviour of an ORC cycle. The model is robust, stable, quick and measures were taken to validate it over a range of external loops conditions.

The development of every component have been paired with a study of the most common simulation approaches found in literature. The more suitable model have been chosen considering the general precision and simplicity, in order to have a reliable and quick system simulation.
Even if the whole model has been constructed around the particular power plant available for the experiments, the method used can be easily applied or extended to any other different WHR application.

The most important result of this work is the development of a map for the analysis of the part-load behaviour. This result can be used to predicted the performance of the ORC over a wide range of operating conditions and opens to a large number of future developments. In fact, this map can be used as a reliable tool in design and performance evaluation.
For example, some applications such as solar, waste heat, and combined heat and power usually work in changing operating conditions so a part-load model is crucial to evaluate the performance of the cycle over a long period of time. Moreover, this tool can be used to select the best heating loop condition and evaluate the feasibility of a particular application.
Also the thermo-economic analysis of the power plant can substantially benefit from the part-load map; the cost and profit evaluation over the long period will become more precise using this approach because the ambient conditions can be taken into account.

Another interesting result obtained is the construction of a versatile and robust heat exchanger model. The approach developed ensures the conver-

gence of the model over a wide range of conditions and can be easily readapted to other conditions. In fact, to simulate another heat exchanger it is sufficient to change the geometry parameters. The plate heat exchanger are common in a countless number of application and even single-phase conditions can be simulated using this approach.
The expander model follows a semi-empirical approach and thus doesn't allows large extrapolation of the results; however it was possible to achieve a really good precision. Moreover, even if some changes are needed, all the volumetric expanders can be modelled using this method.

Further observations can be made on the use of this ORC model to understand the influence of the various parameters. In chapter 5 some remarks have been made on pressure and mass flow rates. These parameters are very important in the determination of the final cost. For example, the best conditions of output power and efficiency correspond to working points with very high evaporating pressure. This condition is likely to require a more expensive design of all the high-pressure elements, representing a strong influence on the economic analysis.

Finally an important achievement that I would like to underline is the professional growth brought by this experience. Even if no particular result can be claimed from this point of view, I think I have learned a lot. First of all, I had the possibility to learn from experienced experts in this field. Moreover, having the possibility to work on a real power plant, I could acquire a greater awareness of these systems.

Concluding the work it is appropriate to resume the limits of this thesis as well. First of all, the behaviour of the ORC's components is described only by static models, so the transient behaviour is not modelled. That is adequate for a long term analysis but it is not suitable for a real-time control strategy.
Moreover, the experimental campaign was quite limited; having the possibility to evaluate the model over a wider range of working points would have improved the reliability of the model.
Some further development could have been made: a thermo-economic evaluation of the components and the analysis of another real-life application would have been a really interesting development of this model. Anyhow this work was quite long and the limits of time quite strict.

# Bibliography


[1] Greenship, 2008. URL http://www.greenship.org.

[2] Euroadmap2050., 2010. URL http://www.roadmap2050.euS.

[3] Iresen 1 mwe csp-orc pilot project, 2015. URL http://www.nrel.gov/csp/solarpaces/project_detail.cfm/projectID=4287.

[4] Swep heat exchangers., 2015. URL http://www.swep.net/products/b200t/.

[5] Wendy C Andersen and Thomas J Bruno. Rapid screening of fluids for chemical stability in organic rankine cycle applications. *Industrial & Engineering Chemistry Research*, 44(15):5560–5566, 2005.

[6] Marco Astolfi, Matteo C Romano, Paola Bombarda, and Ennio Macchi. Binary orc (organic rankine cycles) power plants for the exploitation of medium–low temperature geothermal sources–part b: Techno-economic optimization. *Energy*, 66:435–446, 2014.

[7] Vamshi Krishna Avadhanula and Chuen-Sen Lin. Empirical models for a screw expander based on experimental data from organic rankine cycle system testing. *Journal of Engineering for Gas Turbines and Power*, 136(6):062601, 2014.

[8] O Badr, SD Probert, and PW O'callaghan. Selecting a working fluid for a rankine-cycle engine. *Applied Energy*, 21(1):1–42, 1985.

[9] Owen Bailey and Ernst Worrell. Clean energy technologies: A preliminary inventory of the potential for electricity generation. *Lawrence Berkeley National Laboratory*, 2005.

[10] Junjiang Bao and Li Zhao. A review of working fluid and expander selections for organic rankine cycle. *Renewable and Sustainable Energy Reviews*, 24:325–342, 2013.

[11] Ian H. Bell, Jorrit Wronski, Sylvain Quoilin, and Vincent Lemort. Pure and pseudo-pure fluid thermophysical property evaluation and the open-source thermophysical property library coolprop. *Industrial & Engineering Chemistry Research*, 53(6):2498–2508, 2014. doi: 10.1021/ie4033999. URL `http://pubs.acs.org/doi/abs/10.1021/ie4033999`.

[12] R Bini, A Guercio, and A Duvia. Organic rankine cycle (orc) in biomass applications for cogenerative systems in association with adsorption chillers. In *Proceedings of 5th Dubrovnik Conference on Sustainable Development of Energy, Water and Environment Systems, Dubrovnik, Croatia, Sept*, 2009.

[13] B Blunier, G Cirrincione, Y Herve, and A Miraoui. A new analytical and dynamical model of a scroll compressor with experimental validation. *International Journal of Refrigeration*, 32(5):874–891, 2009.

[14] Aleksandra Borsukiewicz-Gozdur and Władysław Nowak. Maximising the working fluid flow as a way of increasing power output of geothermal power plant. *Applied thermal engineering*, 27(11):2074–2078, 2007.

[15] Roberto Bracco, Stefano Clemente, Diego Micheli, and Mauro Reini. Experimental tests and modelization of a domestic-scale orc (organic rankine cycle). *Energy*, 58:107–116, 2013.

[16] C. Casci, G. Angelino, P. Ferrari, M. Gaia, G. Giglioli, and E. Macchi. Heat recovery in a ceramic kiln with an organic rankine cycle engine. *Journal of Heat Recovery Systems*, 1(2):125 – 131, 1981. ISSN 0198-7593. doi: http://dx.doi.org/10.1016/0198-7593(81)90027-8. URL `http://www.sciencedirect.com/science/article/pii/0198759381900278`.

[17] Huijuan Chen, D Yogi Goswami, and Elias K Stefanakos. A review of thermodynamic cycles and working fluids for the conversion of low-grade heat. *Renewable and sustainable energy reviews*, 14(9):3059–3067, 2010.

[18] Yu Chen, Nils P Halm, Eckhard A Groll, and James E Braun. Mathematical modeling of scroll compressors, part i: compression process modeling. *International Journal of Refrigeration*, 25(6):731–750, 2002.

[19] Sébastien Declaye, Sylvain Quoilin, Ludovic Guillaume, and Vincent Lemort. Experimental study on an open-drive scroll expander integrated into an orc (organic rankine cycle) system with r245fa as working fluid. *Energy*, 55:173–183, 2013.

[20] Agustín M Delgado-Torres. Solar thermal heat engines for water pumping: An update. *Renewable and Sustainable Energy Reviews*, 13(2): 462–472, 2009.

[21] Nishith B Desai and Santanu Bandyopadhyay. Process integration of organic rankine cycle. *Energy*, 34(10):1674–1686, 2009.

[22] Ronald DiPippo. *Geothermal power plants: principles, applications, case studies and environmental impact*. Butterworth-Heinemann, 2012.

[23] Leilei Dong, Hao Liu, and Saffa Riffat. Development of small-scale and micro-scale biomass-fuelled chp systems–a literature review. *Applied thermal engineering*, 29(11):2119–2126, 2009.

[24] Tsuneo Endo, Shogo Kawajiri, Yoichi Kojima, Kazuya Takahashi, Tsuyoshi Baba, Shigeru Ibaraki, Tsutomu Takahashi, and M Shinohara. Study on maximizing exergy in automotive engines. Technical report, SAE Technical Paper, 2007.

[25] Karen Anne Finney. Ocean thermal energy conversion. *Guelph Engineering Journal*, 1:17–23, 2008.

[26] Alessandro Franco and Marco Villani. Optimal design of binary cycle power plants for water-dominated, medium-temperature geothermal fields. *Geothermics*, 38(4):379–391, 2009.

[27] Zhaolin Gu and Haruki Sato. Performance of supercritical cycles for geothermal binary design. *Energy Conversion and Management*, 43(7): 961–971, 2002.

[28] Dong-Hyouck Han, Kyu-Jung Lee, and Yoon-Ho Kim. The characteristics of condensation in brazed plate heat exchangers with different chevron angles. *JOURNAL-KOREAN PHYSICAL SOCIETY*, 43(1): 66–73, 2003.

[29] Dong-Hyouck Han, Kyu-Jung Lee, and Yoon-Ho Kim. Experiments on the characteristics of evaporation of r410a in brazed plate heat exchangers with different geometric configurations. *Applied thermal engineering*, 23(10):1209–1225, 2003.

[30] HD Madhawa Hettiarachchi, Mihajlo Golubovic, William M Worek, and Yasuyuki Ikegami. Optimum design criteria for an organic rankine cycle using low-temperature geothermal heat sources. *Energy*, 32(9):1698–1706, 2007.

[31] Sung-Wei Hsu, Hsiao-Wei D Chiang, and Chih-Wei Yen. Experimental investigation of the performance of a hermetic screw-expander organic rankine cycle. *Energies*, 7(9):6172–6185, 2014.

[32] Tzu-Chen Hung, TY Shai, and SK Wang. A review of organic rankine cycles (orcs) for the recovery of low-grade waste heat. *Energy*, 22(7): 661–667, 1997.

[33] Muhyiddine Jradi, Jinxing Li, Hao Liu, and Saffa Riffat. Micro-scale orc-based combined heat and power system using a novel scroll expander. *International Journal of Low-Carbon Technologies*, page ctu012, 2014.

[34] El Hadj Malick Kane, Daniel Favrat, Benoit Gay, and O Andres. Scroll expander organic rankine cycle (orc) efficiency boost of biogas engines. In *Ecos 2007*, volume 2, pages 1017–1024. Università degli Studi Di Padova, 2007.

[35] Ahmed Kovacevic, Nikola Stosic, Ian Keneth Smith, and Elvedin Mujic. Advances in numerical modelling of helical screw machines. 2010.

[36] Jaakko Larjola. Electricity from industrial waste heat using high-speed organic rankine cycle (orc). *International journal of production economics*, 41(1):227–235, 1995.

[37] Steven Lecompte, Henk Huisseune, Martijn van den Broek, Sven De Schampheleire, and Michel De Paepe. Part load based thermo-economic optimization of the organic rankine cycle (orc) applied to a combined heat and power (chp) system. *Applied Energy*, 111:871–881, 2013.

[38] Steven Lecompte, Henk Huisseune, Martijn van den Broek, Bruno Vanslambrouck, and Michel De Paepe. Review of organic rankine cycle (orc) architectures for waste heat recovery. *Renewable and Sustainable Energy Reviews*, 47:448–461, 2015.

[39] H Leibowitz, IK Smith, and N Stosic. Cost effective small scale orc systems for power recovery from low grade heat sources. In *ASME 2006 International Mechanical Engineering Congress and Exposition*, pages 521–527. American Society of Mechanical Engineers, 2006.

[40] Vincent Lemort, Sylvain Quoilin, Cristian Cuevas, and Jean Lebrun. Testing and modeling a scroll expander integrated into an organic rankine cycle. *Applied Thermal Engineering*, 29(14):3094–3102, 2009.

[41] Vincent Lemort, Sébastien Declaye, and Sylvain Quoilin. Experimental characterization of a hermetic scroll expander for use in a micro-scale rankine cycle. *Proceedings of the Institution of Mechanical Engineers, Part A: Journal of Power and Energy*, 226(1):126–136, 2012.

[42] Hao Liu, Yingjuan Shao, and Jinxing Li. A biomass-fired micro-scale chp system with organic rankine cycle (orc)–thermodynamic modelling studies. *Biomass and Bioenergy*, 35(9):3985–3994, 2011.

[43] V Macián, JR Serrano, V Dolz, and J Sánchez. Methodology to design a bottoming rankine cycle, as a waste energy recovering system in vehicles. study in a hdd engine. *Applied Energy*, 104:758–771, 2013.

[44] V Maizza and A Maizza. Working fluids in non-steady flows for waste energy recovery systems. *Applied Thermal Engineering*, 16(7):579–590, 1996.

[45] Holger Martin. A theoretical approach to predict the performance of chevron-type plate heat exchangers. *Chemical Engineering and Processing: Process Intensification*, 35(4):301–310, 1996.

[46] Guilherme Leibsohn Martins, Sergio Leal Braga, and Sandro Barros Ferreira. Design optimization of partial admission axial turbine for orc service. *Applied Thermal Engineering*, 96:18–25, 2016.

[47] James A Mathias, Jon R Johnston, Jiming Cao, Douglas K Priedeman, and Richard N Christensen. Experimental testing of gerotor and scroll expanders used in, and energetic and exergetic modeling of, an organic rankine cycle. *Journal of Energy Resources Technology*, 131(1):012201, 2009.

[48] Hans B Pacejka. Tyre and vehicle dynamics, 2002. *Butterworth-Heinemann, ISBN 0*, 7506(5141):5, 2006.

[49] Iva Papes, Joris Degroote, and Jan Vierendeels. New insights in twin screw expander performance for small scale orc systems from 3d cfd analysis. *Applied Thermal Engineering*, 91:535–546, 2015.

[50] Gang Pei, Jing Li, Yunzhu Li, Dongyue Wang, and Jie Ji. Construction and dynamic test of a small-scale organic rankine cycle. *Energy*, 36(5): 3215–3223, 2011.

[51] Guoquan Qiu, Hao Liu, and Saffa Riffat. Expanders for micro-chp systems with organic rankine cycle. *Applied Thermal Engineering*, 31(16): 3301–3307, 2011.

[52] Sylvain Quoilin, Sébastien Declaye, Bertrand F Tchanche, and Vincent Lemort. Thermo-economic optimization of waste heat recovery organic rankine cycles. *Applied Thermal Engineering*, 31(14):2885–2893, 2011.

[53] Sylvain Quoilin, Martijn Van Den Broek, Sébastien Declaye, Pierre Dewallef, and Vincent Lemort. Techno-economic survey of organic rankine cycle (orc) systems. *Renewable and Sustainable Energy Reviews*, 22: 168–186, 2013.

[54] Takeo Saitoh, Noboru Yamada, and Shin-Ichiro Wakashima. Solar rankine cycle system using scroll expander. *Journal of Environment and Engineering*, 2(4):708–719, 2007.

[55] A Schuster, S Karellas, E Kakaras, and H Spliethoff. Energetic and economic investigation of organic rankine cycle applications. *Applied thermal engineering*, 29(8):1809–1817, 2009.

[56] Ramesh K Shah and Dusan P Sekulic. *Fundamentals of heat exchanger design*. John Wiley & Sons, 2003.

[57] Zhang Shengjun, Wang Huaixin, and Guo Tao. Performance comparison and parametric optimization of subcritical organic rankine cycle (orc) and transcritical power cycle system for low-temperature geothermal power generation. *Applied energy*, 88(8):2740–2754, 2011.

[58] Ian K Smith, N Stošič, and CA Aldis. Development of the trilateral flash cycle system: Part 3: The design of high-efficiency two-phase screw expanders. *Proceedings of the Institution of Mechanical Engineers, Part A: Journal of Power and Energy*, 210(1):75–93, 1996.

[59] Ian K Smith, Nikola Stosic, and Ahmed Kovacevic. Power recovery from low cost two-phase expanders. *Transactions-Geothermal Resources Council*, pages 601–606, 2001.

[60] Panpan Song, Mingshan Wei, Lei Shi, Syed Noman Danish, and Chaochen Ma. A review of scroll expanders for organic rankine cycle systems. *Applied Thermal Engineering*, 75:54–64, 2015.

[61] William Stine and Michael Geyer. *Power From The Sun*. John Wiley and Sons.

[62] Bertrand F Tchanche, Gr Lambrinos, Antonios Frangoudakis, and George Papadakis. Low-grade heat conversion into power using organic rankine cycles–a review of various applications. *Renewable and Sustainable Energy Reviews*, 15(8):3963–3979, 2011.

[63] Hua Tian, Gequn Shu, Haiqiao Wei, Xingyu Liang, and Lina Liu. Fluids and parameters optimization for the organic rankine cycles (orcs) used in exhaust heat recovery of internal combustion engine (ice). *Energy*, 47 (1):125–136, 2012.

[64] Bryant Tyler. Energy efficiency market report, 2015.

[65] Iacopo Vaja and Agostino Gambarotta. Internal combustion engine (ice) bottoming with organic rankine cycles (orcs). *Energy*, 35(2):1084–1093, 2010.

[66] Brandon J Woodland, James E Braun, Eckhard A Groll, and W Travis Horton. Experimental testing of an organic rankine cycle with scroll-type expander. 2012.

[67] Robert Zanelli and Daniel Favrat. Experimental investigation of a hermetic scroll expander-generator. 1994.

[68] HG Zhang, EH Wang, and BY Fan. A performance analysis of a novel system of a dual loop bottoming organic rankine cycle (orc) with a light-duty diesel engine. *Applied Energy*, 102:1504–1513, 2013.